265A

TECHNICAL REPORT

JOINT INDUSTRY PROJECT

RELIABILITY OF CORRODED PIPES
FINITE ELEMENT ANALYSES

REPORT NO. 96-3392

REVISION NO. 01

DET NORSKE VERITAS

Table of Contents

1 CONCLUSIVE SUMMARY

This report is one in a series of 4 reports in the JIP project "Reliability of Corroded Pipes". The objective of the project has been to provide burst capacity and acceptance formulas with consistent reliability levels for corroded pipes.

The work includes a series of laboratory tests and a large number of FE analyses of corroded pipes exposed to internal pressure and combined internal pressure and external compressive loading. Both longitudinal and circumferential corrosion are considered.

This report describes the finite element analyses of pipes with simulated smooth corrosion defects.

A large number of finite element analyses were performed to estimate the burst capacity of corroded pipes covering variations in parameters as the pipe diameter, the wall thickness, length and depth of the corrosion defect, shape of the corrosion defect, combined loading and material properties. Both longitudinal corrosion and circumferential corrosion defects were included in the study.

In this report the analyses are described, which includes description of the models, the parameters studied, the solution strategies, etc. and the main conclusions. The failure criterion for the analyses with applied internal pressure was adopted from the work by British Gas (Fu and Kirkwood), and a strain criterion was applied for the analyses with combined loads.

The analyses, in combination with the laboratory tests performed within the project, forms the background for the development of the capacity equation and the calibrated design equation for corroded pipes, which is described in the project report "Reliability of Corroded Pipes, Assessment of Capacity and Acceptance Criteria."

2 INTRODUCTION

2.1 Motivation

A pipeline is a large financial asset for the pipeline operator and a safe operation of the pipeline is therefore of great concern. On the other hand, unnecessary repair and an over conservative operation of the pipeline may result in high costs and unexploded resource utilisation. As the pipelines are ageing and corrosion may develop, the economical consequences of reduced operation pressure, repairs, or replacements may become high.

Existing design codes for burst strength assessment of corroded pipes have a inconsistent safety level for varying degree of corrosion, which may result in both hazardous designs or possibly costly and unrequired requalification actions. Available acceptance equations for assessment of allowable operating pressures of degraded pipelines depending on the selected reliability level are therefore desirable.

When severe corrosion has been observed in a pipeline, the selection of required action to be carried out should be based on an overall assessment of the pipeline, where uncertainties associated with both the assessment of the degree of corrosion and the capacity evaluation should be considered. Repair or replacement of the pipeline should be avoided, or postponed in time, if this is possible within the safety requirements defined. Required actions should further also be initiated in order to maintain the integrity of the pipeline and to avoid an undesired risk exposure of the pipeline.

2.2 Background

The present Joint Industry Project "*Reliability of Corroded Pipes*" is a continuation of the project "*Residual Strength of Corroded and Dented Pipes*". The former project, Phase I, was started in 1993 and concluded at the end of 1995. The present project, Phase II, stared shortly after.

The Phase I of the project was sponsored by Statoil, Phillips, Brasoil (Petrobras), Mineral Management Services (MMS), Norwegian Petroleum Directorate (NPD), The Research Council of Norway (NFR), and Det Norske Veritas (DNV).

The Phase II of the project "*Reliability of Corroded Pipes*" is sponsored by Statoil, Amoco, Exxon, NPD, MMS and Brasoil (Petrobras).

The project scope of work has been modified during the course of the project to better utilise the funding. Especially, the work conducted by British Gas in a corresponding project has had an impact on the course of this project.

To avoid unnecessary overlapping, the initial scope was changed to covering the development of capacity and acceptance equations for combined internal pressure and external loading for both longitudinal corrosion and circumferential corrosion, where the acceptance equation for longitudinal corrosion was based on a probabilistic calibration. The basis for such a development was a series of finite element analysis and a reduced series of laboratory test compared to the initial scope.

British Gas had prior to the initiation of Phase II of the project performed several laboratory tests and finite element analyses for internal pressure only, accounting also for the interaction of separate pits and grooves. However, this work would not include a probabilistic calibration of an acceptance (design) equation. A merging of the outcome from the DNV and the British Gas projects would therefore be natural.

The advantage with a co-operation between the DNV and the British Gas projects would be that the obtained capacity and acceptance equations in the DNV project could be calibrated to a larger database. A set of common recommended capacity and acceptance design equations from the DNV and British Gas projects could then be proposed, which would also likely receive a higher recognition in the marked.

Such a co-operation could be initiated after the completion of both the DNV and the British Gas projects, by the development of a unified guideline for burst of corroded pipes.

2.3 Project Reports

The project concludes with the reports defined in Table 2-1.

Table 2-1 Overview of the project reports

DNV report no.	Title / Subject
96-3392	Reliability of Corroded Pipes / Finite Element Analyses
96-3393	Reliability of Corroded Pipes / Laboratory Burst Tests
96-3394	Reliability of Corroded Pipes / Assessment of Capacity and Acceptance Criteria
97-3358	Reliability of Corroded Pipes / Project Guideline

2.4 Participants and their Representatives

The following organisations participated in the project;

Participant	Representative	Telephone / Fax	
Minerals Management Service (MMS)	Wallace O. Adcox	Telephone Fax	(+1) 703 787 1354 (+1) 703 787 1010
Norwegian Petroleum Directorate (NPD)	Kjell A. Anfinsen	Telephone Fax	(+47) 51 87 62 26 (+47) 51 55 15 71
Den norske stats oljeselskap a.s.(Statoil)	Richard Verley	Telephone Fax	(+47) 73 58 41 85 (+47) 73 96 72 86
Amoco Norway Oil Company (Amoco)	Ole Jørgen Narvestad	Telephone Fax	(+47) 51 50 20 18 (+47) 51 50 22 18
Exxon Production Research Company (EPR)	Robert Appleby	Telephone Fax	(+1) 713 965 7193 (+1) 713 966 6423
Petrobras /CENPES/DIPREX	Adilson C. Benjamin	Telephone Fax	(+55) 21 598 6263 (+55) 21 598 6793

2.5 Conversion Factors

SI units are used in the report. The conversion factors between SI units and US units are;

From US units to SI units

Length:	1 in (inch)	=	25.40 mm
Mass	1 lb (pound)	=	0.4536 kg
Force	1 lbf (pound force)	=	4.448 N
	1 kip	=	4.448 kN
Stress (Pressure)	1 psi (lbf/in2)	=	0.006895 MPa (N/mm2)
	1 ksi (1000 psi)	=	6.895 Mpa

From SI units to U. S units

Length:	1 mm	=	0.03937 in
Mass	1 kg	=	2.205 lb (pound)
Force	1 N	=	0.2248 lbf (pound force)
	1 kN	=	0.2248 kip
Stress (Pressure)	1 Mpa	=	145.0 psi (lbf/in2)
	1 Mpa	=	0.1450 ksi

1 ksi = 1000 psi

10 bar = 1 MPa

3 GENERAL INFORMATION OF THE MODELS AND ANALYSES

3.1 Introduction

A large number of analyses have been carried out with various pipe wall thickness and extent of corrosion defects, and different loading conditions and material properties have been applied. Approximately 100 models were generated (different pipe dimensions and corrosion defect), and the models were analysed with various loading conditions and material properties, resulting in a few hundred analyses.

Most of the models were 3D models with solid elements and full non-linear material and geometry formulation. When appropriate, as for instance this was applied for the analyses of the girth weld corrosion, 2D models were used. In this specific case axisymmetric plane solid elements were applied. Also the burst capacity of none and infinite long corrosion defect were analysed using 2D models, and in this case plane strain elements were applied.

The FE analyses were carried out using the general purposed non-linear program ABAQUS version 5.4 and 5.5, on a VAX Alpha 2100 4/275 computer. The solution time for the 2D analyses varied from a few seconds to some minutes and from 20 minutes to 15 hours for the 3D models. The total CPU time used is approximately 700 hours.

3.2 Overview of the FE models

The majority of the 3D models were generated with outer pipe diameter of 324 mm (D), with 3 different wall thickness (t), 10mm, 16mm and 22mm and various extent of corrosion defects. The models were selected to cover the following basic parameters;

- Diameter: 324 mm
- Thickness 10, 16 and 22 mm (D/t ratio of 32, 20 and 15)
- Corrosion defect depth 0.15, 0.30, 0.50 and 0.70 of the wall thickness
- Corrosion defect length 0.15, 0.25, 0.50, 0.75, 1.0, and 2.0 of the pipe diameter

For the full matrix of the pipe and defect dimensions given above, a total of 72 models were generated. Additional 3D models has been generated with deeper or wider corrosion, internal versus external corrosion, and a few models were made in order to duplicate published results in order to validate the results. The corrosion defects were rectangular shape with smooth edges. A few models with parabolic corrosion defect shape were generated.

The girth weld corrosion defects were analysed employing axisymmetric 2D models. Likewise, the effect of the corrosion defect width of longitudinal defects with infinity length was assessed using plane strain 2D models. The effect of the shape of transition between the plain pipe and the corrosion defect for infinity long corrosion were also studied, as well as the effect of various mesh densities were also studied using 2D models.

All defects assessed were single smooth shaped corrosion defects.

Selected plots of the models are show in Figure 3-3 to Figure 3-11.

3.3 Computer program

The general purpose no-linear program ABAQUS, version 5.4 and 5.5 was used.

3.4 Generation of the models

The FE element models were generated in Solvia-Pre, and the node co-ordinates, element topology, boundary conditions and pressure load were converted to ABAQUS input format by use of an in-house program. The additional input required for the analyses were edited into the ABAQUS input file, such as material properties, loading sequence etc..

3.5 Mesh and element types

For the all the 3D models the solid element C3D20R were used. This is a reduced integration order 20 noded element. In the corroded region 4 elements were used through the thickness, and at some distance away from the corroded region the number of elements were reduced to 1 element through the thickness.

For the 2D modes the solid element types CAX8R and CPE8R was used for axi-symmetric and plain strain analyses, respectively.

Typical size of a 2D model was 500 nodes and 100 elements. Number of degree of freedom (in ABAQUS noted variables) were 800, and wavefront approximately 30.

Typically for the 3D models the size of the models varied from 2500 to 8000 nodes, and from 350 to 1300 elements. Number of variables varied from 7000 to 22000, and wavefront from 250 to 600.

3.6 Boundary conditions

For the 3D models advantage of symmetry was taken, hence only 1/4 of the pipe was modelled. Symmetry boundary conditions were applied at the symmetry planes.

For the models with internal pressure and bending moment additional boundary conditions were applied at the end of the pipe, and a beam element were connected to the end to allow for application of bending moment or prescribed rotation.

3.7 Loads

Internal pressure was applied at all internal surfaces of the pipe. The axial tension due to the end cap was applied in the pipe wall at the cut-off boundary of the model simultaneously with the internal pressure. For the full non-linear analyses the surface pressure loads are also updated with updated geometry due to deformations. This is vital for the burst capacity analyses, and in case of not updating both the geometry and the loads would have given erroneous results.

Models to which bending moment were applied were made with a beam at the boundaries of the model for easy application and control of the bending moment. The axial compressive loads were applied at the cut-off boundary of the model.

3.8 Materials

The material properties were based on the results from the Superb project, giving the mean values and the distribution for the material yield and tensile strength for different materials from X60 to X80. For the purpose of the finite element analyses the material curve is required given in true stress versus true strain. In order to have a clear definition of the material a procedure to generate different materials were made. By using this procedure and the mean values from the Superb project the "average" X60 material and X80 material were generated.

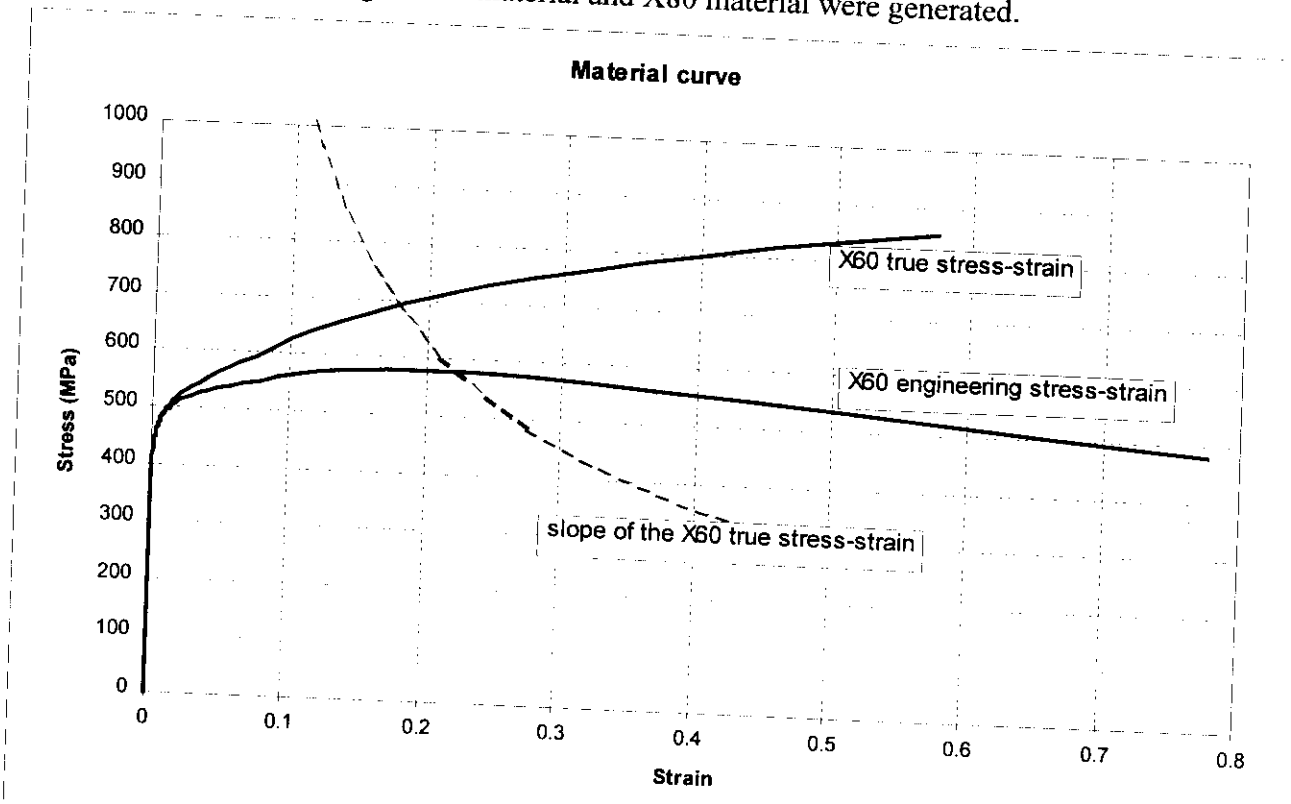

Figure 3-1 True and engineering stress strain material curve for mean X60 material

The true UTS is calculated from the maximum point at the engineering stress-strain curve, using the following expressions;

$$\varepsilon_{true} = \ln(1+\varepsilon_{eng})$$

$$\sigma_{true} = \sigma_{eng}(1+\varepsilon_{eng})$$

This is also the location where the slope of true stress-strain curve is equal to the true-stress strain curve, see figure

The sensitivity of the material properties was also studied, and sets of variations of the X60 material were generated. From the mean yield strength and the mean ultimate strength a ± 10% variation were made, resulting in 9 combinations as listed in Table 3-1. The corresponding 9 material true-stress curves are shown in Figure 3-2

Table 3-1 X60 material variations (engineering values)

X 60 material	+ 10 %	mean value	- 10 %
Yield strength (MPa)	414	460	506
Tensile strength (MPa)	520	578	636

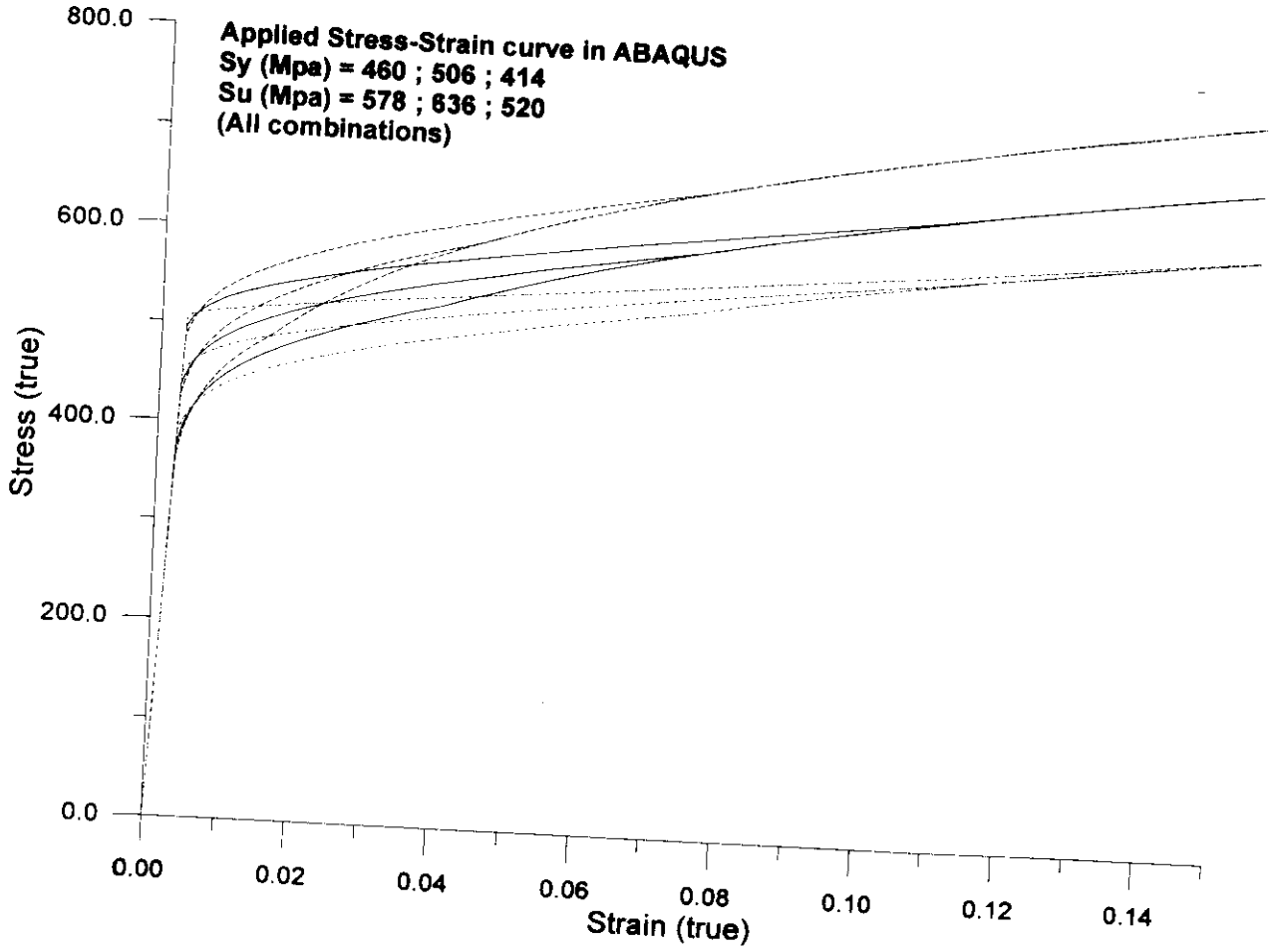

Figure 3-2 True stress-strain material curve for the X60 material sensitivity study

3.9 Solution strategies

The general purpose program ABAQUS was applied for the analyses, and both material non-linearity and non-linear geometry (large deformations) accounted for in all the analyses. In generally a static loading procedure war applied, and the loading was increased until equilibrium was not obtained for a small increment of the applied load.

In ABAQUS a arc-length type of solution strategy called the Riks algorithms is available, which will allow for analyses with an unstable behaviour. By applying this method the loading can continue also after the critical load has been reached, and the load will be decreased allowing further increased deformations. The maximum, or say critical pressure, when using the Riks

method is the same as when the static analysis procedure has become numerically unstable, no equilibrium is obtained.

3.10 Failure criteria

3.10.1 Analyses with internal pressure

The failure criterion for the analyses with applied internal pressure was adopted from the work by British Gas (Fu and Kirkwood, 1995). British Gas has supported and verified the criterion with several unpublished full scale laboratory tests.

In simple terms, burst failure occur when the whole thickness at the corrosion defect has reached UTS, the true stress level at the engineering material tensile strength. For most of the analyses, depending of the size of the corrosion defect, numerical instability occurred at a slightly higher pressure then the failure criterion used.

3.10.2 Analyses with combined loading

The same criterion as for the analyses with internal pressure was not found to be suitable for the analyses with combined loads. There is a significant difference in the local stress distribution in the area of the corrosion defect for a pipe exposed to internal pressure and combined internal pressure and axial compressive loads. For internal pressure only (with end cap), the pipe material is subjected to hoop stress in tension and an axial tensile stress which is half the hoop stress, and the loading is in one direction until failure. Numerical instability will occur at a slightly higher pressure level then the defined failure criteria.

For the case with combined internal pressure and axial compressive force the stress distribution in the area of the corrosion defect is different, and when applying one load only and keeping the other constant, the ratio between the hoop stress and the axial stress changes. And at a high level of compressive stress and a lower level of tensile hoop stress the material will not fail in the hoop direction (burst), but plastically deform. In order to obtain burst the internal pressure has to be increased, and in displacement control due to yielding this will result in reduced reacting axial force. Different failure criteria for the combined loading have been applied. Candidate failure models are for internal pressure only (reached UTS), a strain criterion, a stress criterion, or numerical instability. The latter must be used with care since instability could be caused by improper boundaries of the FE model. For modest axial load the failure criteria where the whole ligament reaches UTS could be appropriate, but for large axial loads and modest internal pressure a strain criteria could be better. In many cases the predicted capacity is not very sensitive to the failure criterion used, as far as the strain level and stress level used as the criterion is adequate. The criterion used is indicated in each case for the analyses with combined load.

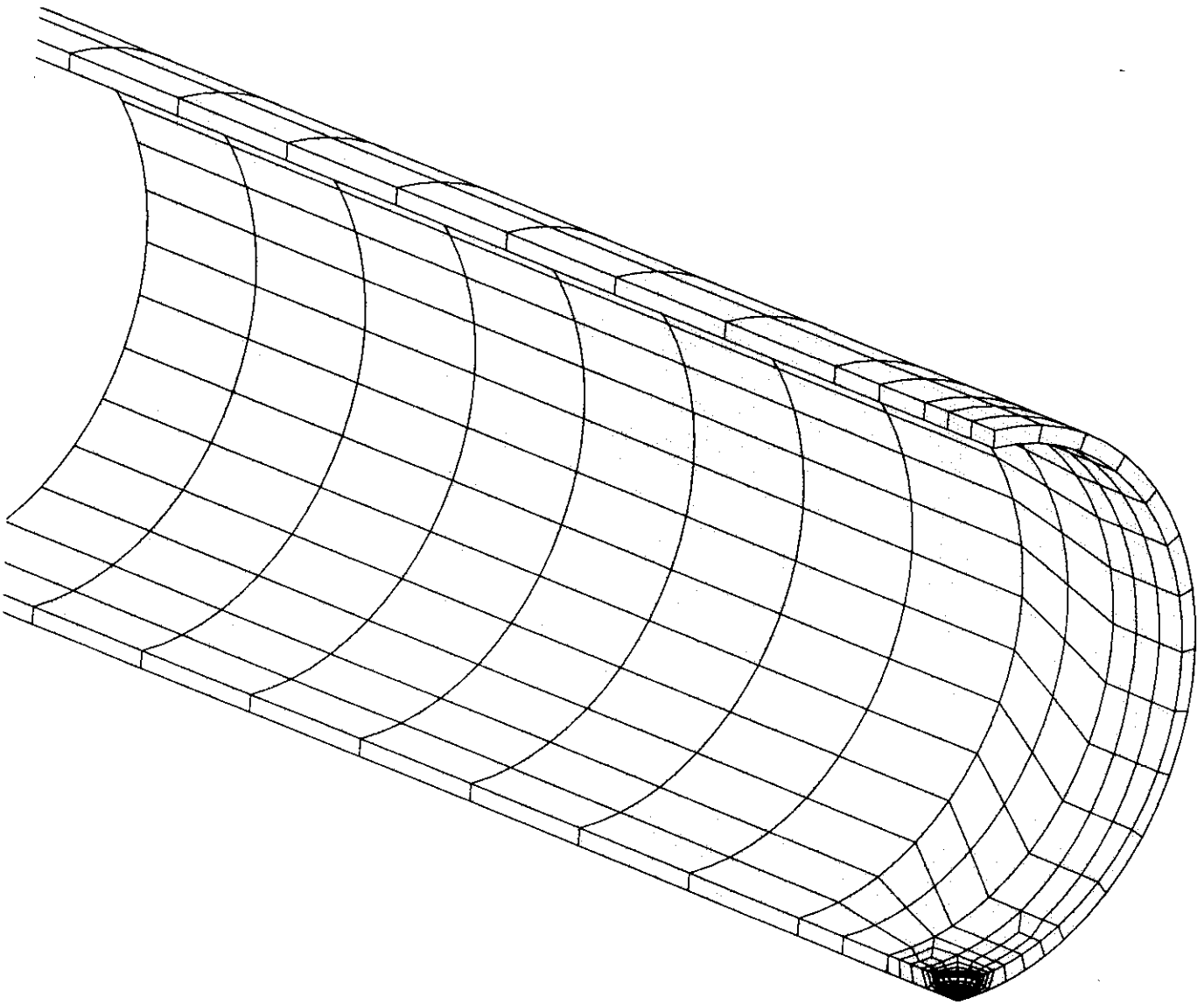

Figure 3-3 Example of typical finite element model, general view. D = 324 mm, t = 10.0 mm, d/t= 0.5, L/D = 0.15, w=3t

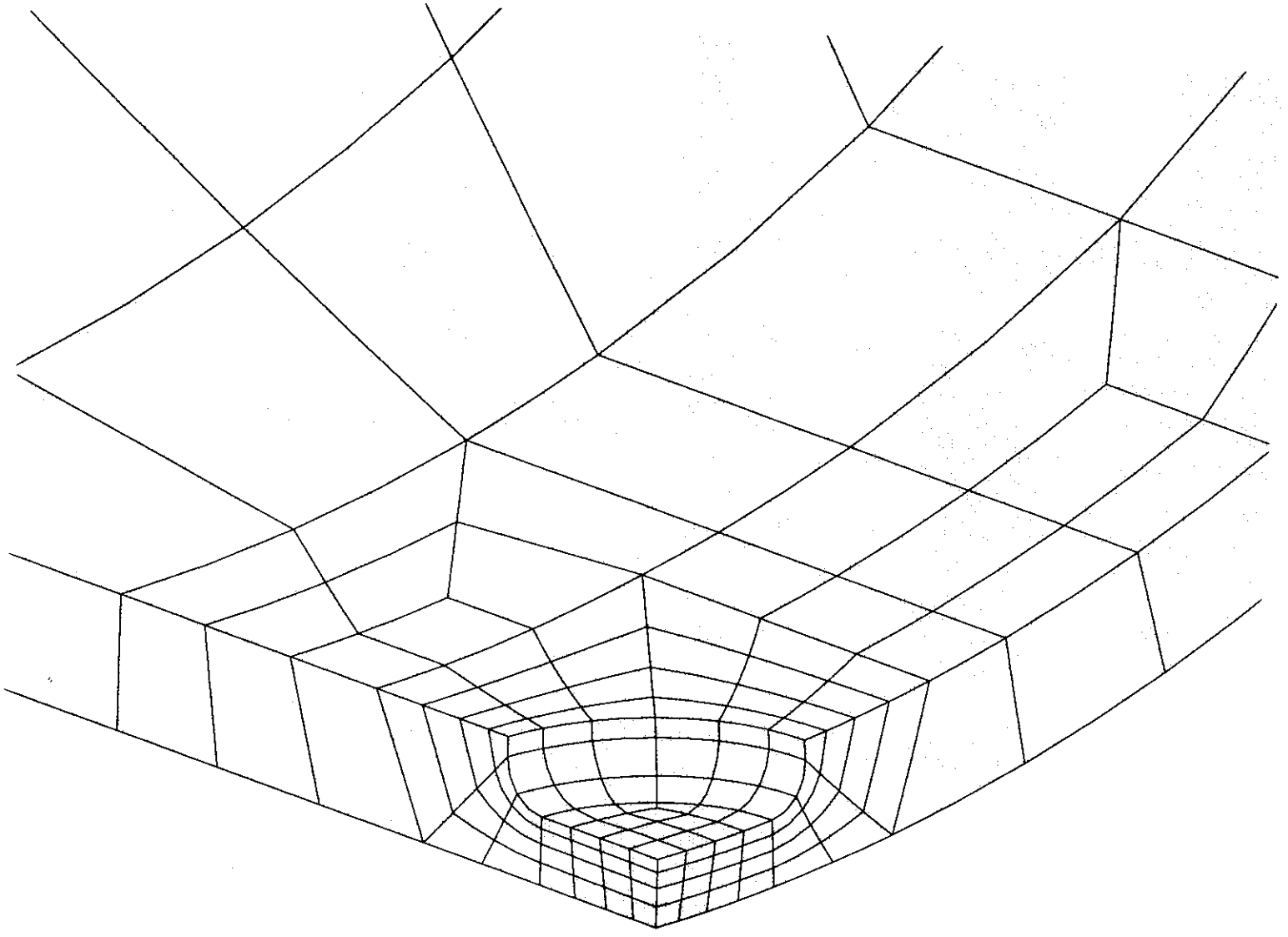

Figure 3-4 Example of typical finite element model, close-up view. D = 324 mm, t = 10.0 mm, d/t= 0.5, L/D = 0.15, w=3t

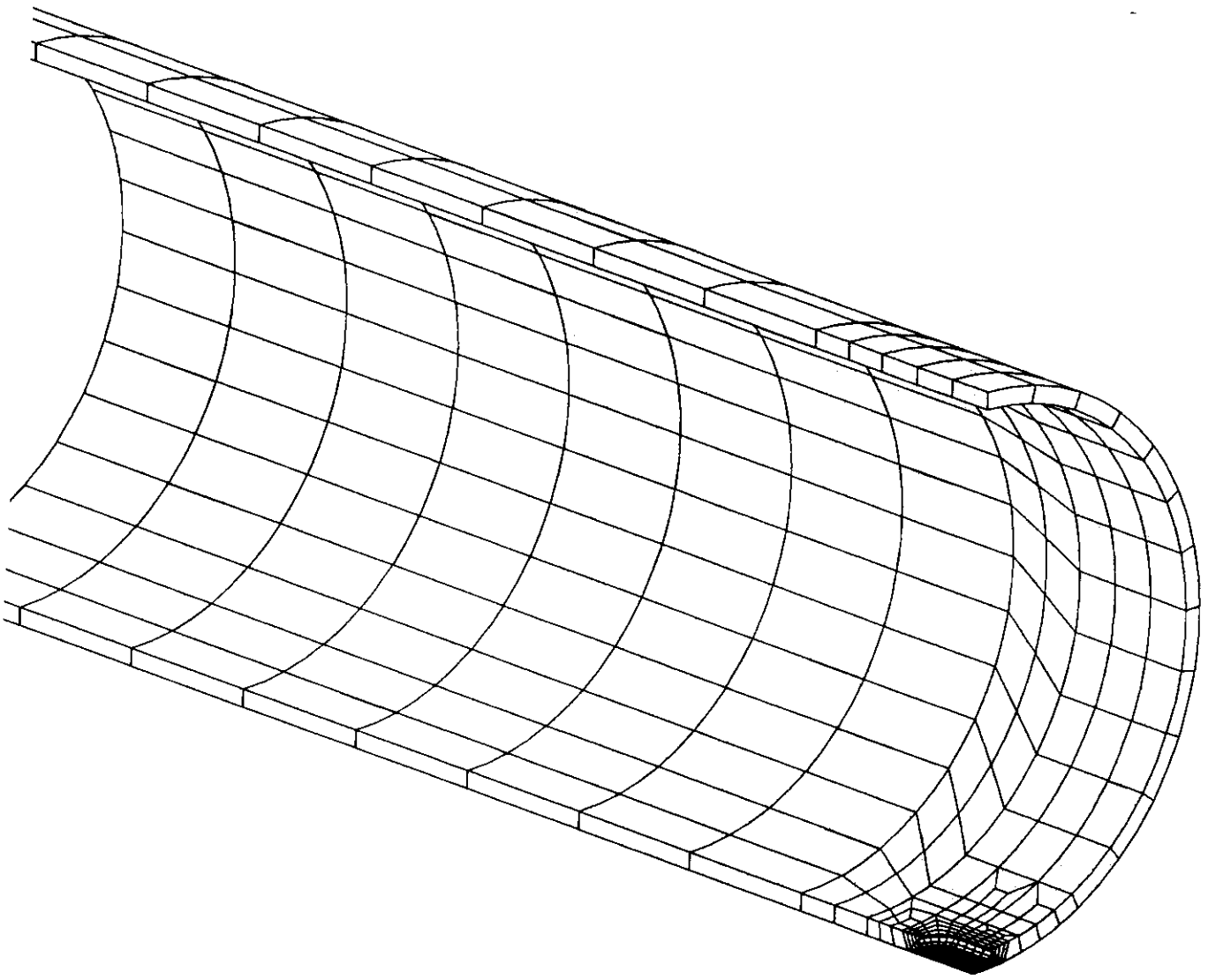

Figure 3-5 Example of typical finite element model, general view. D = 324 mm, t = 10.0 mm, d/t= 0.5, L/D = 0.25, w=3t

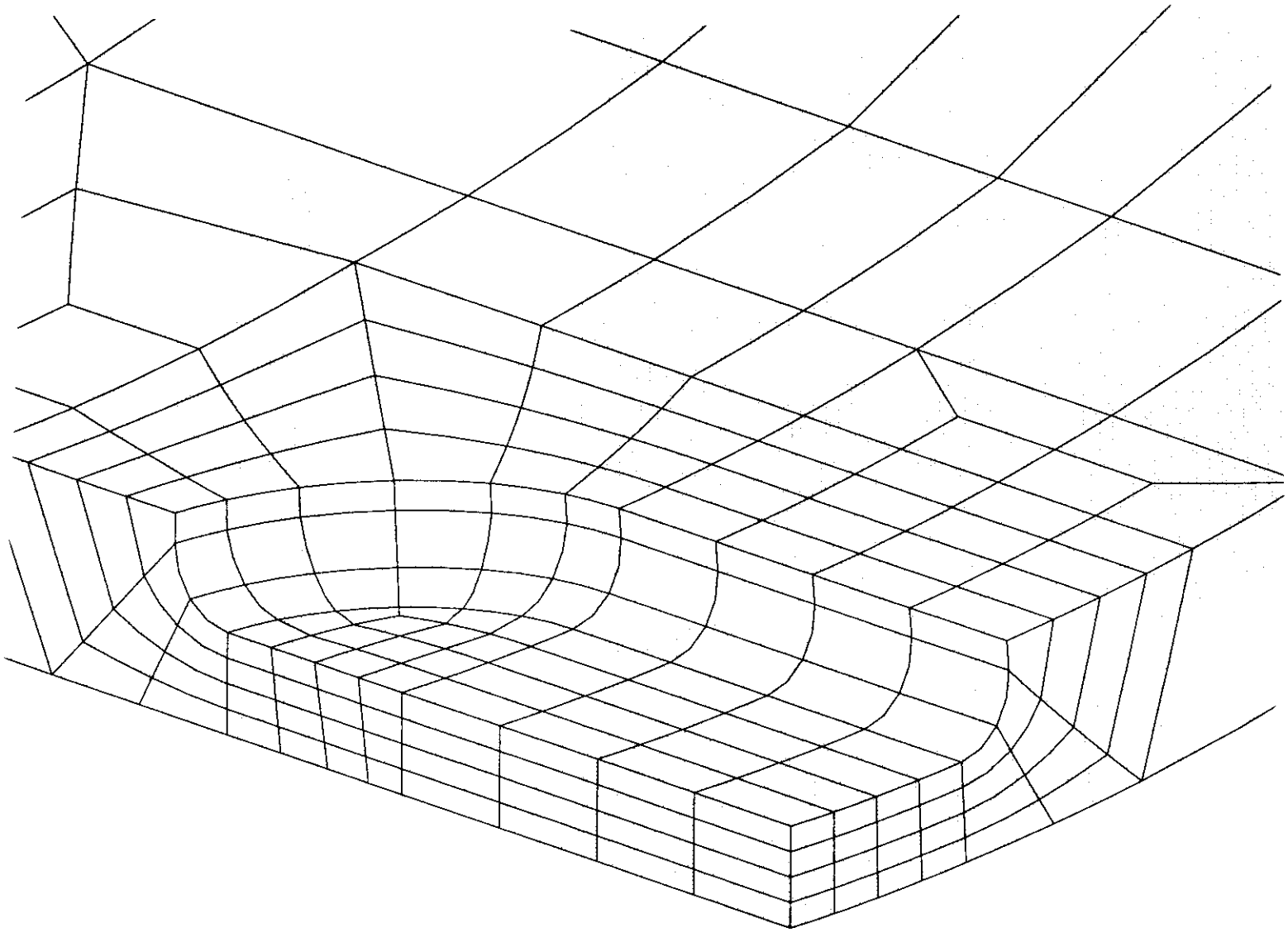

Figure 3-6 Example of typical finite element model, close-up view. D = 324 mm, t = 10.0 mm, d/t= 0.5, L/D = 0.25, w=3t

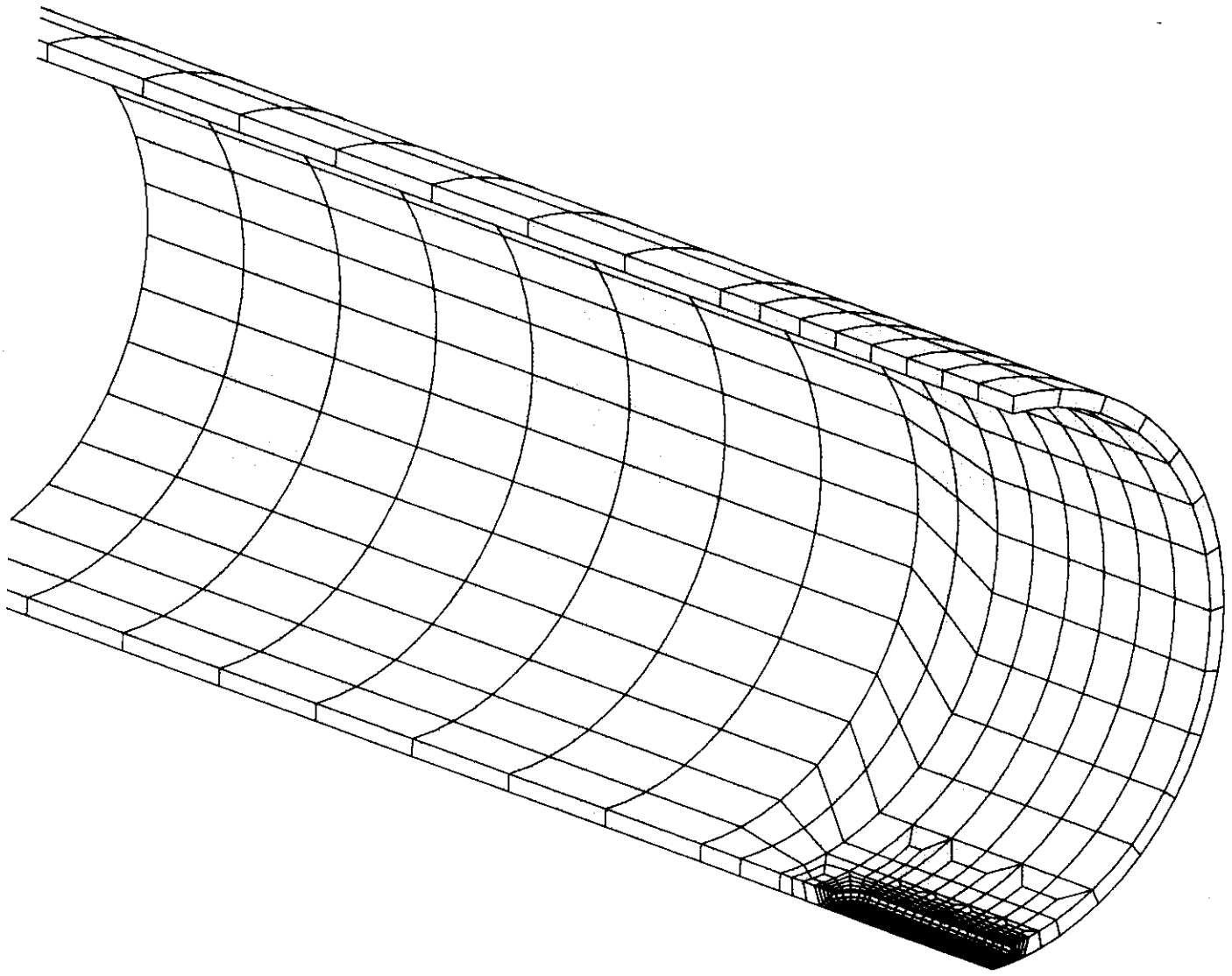

Figure 3-7 Example of typical finite element model, general view. D = 324 mm, t = 10.0 mm, d/t= 0.5, L/D = 0.75, w=3t

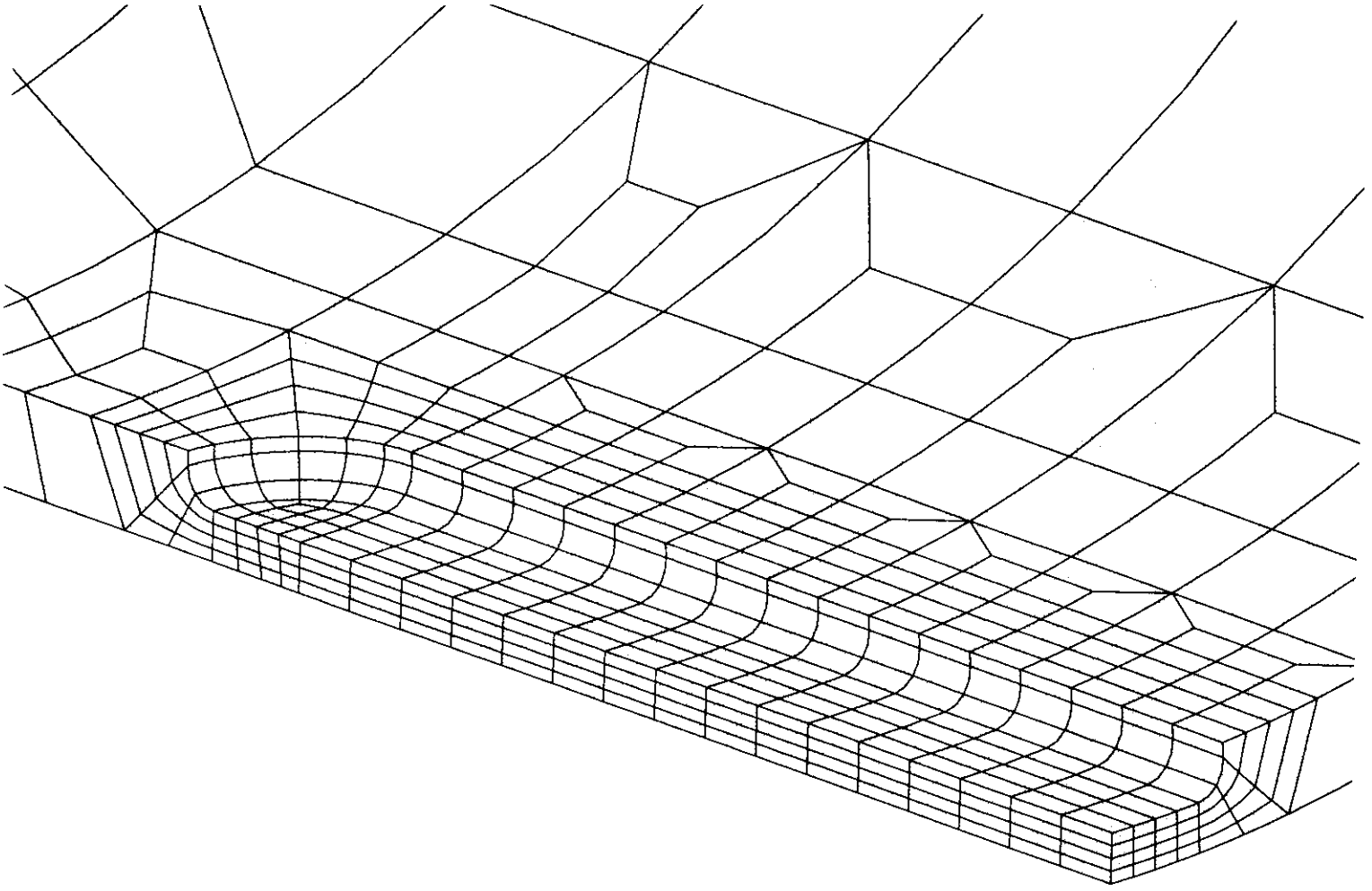

Figure 3-8 Example of typical finite element model, close-up view. D = 324 mm, t = 10.0 mm, d/t= 0.5, L/D = 0.75, w=3t

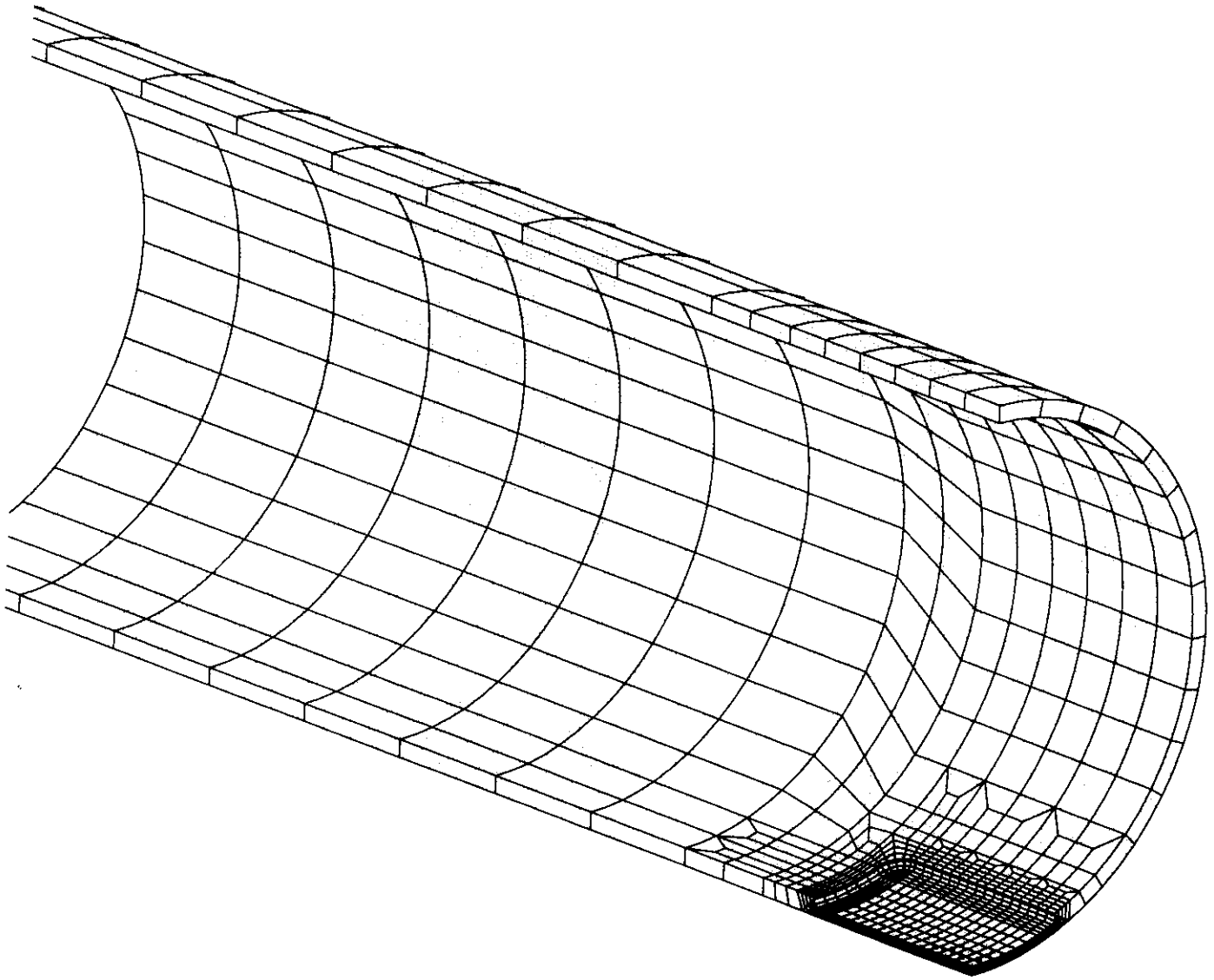

Figure 3-9 Example of typical finite element model, general view. D = 324 mm, t = 10.0 mm, d/t= 0.5, L/D = 0.75, w=15t

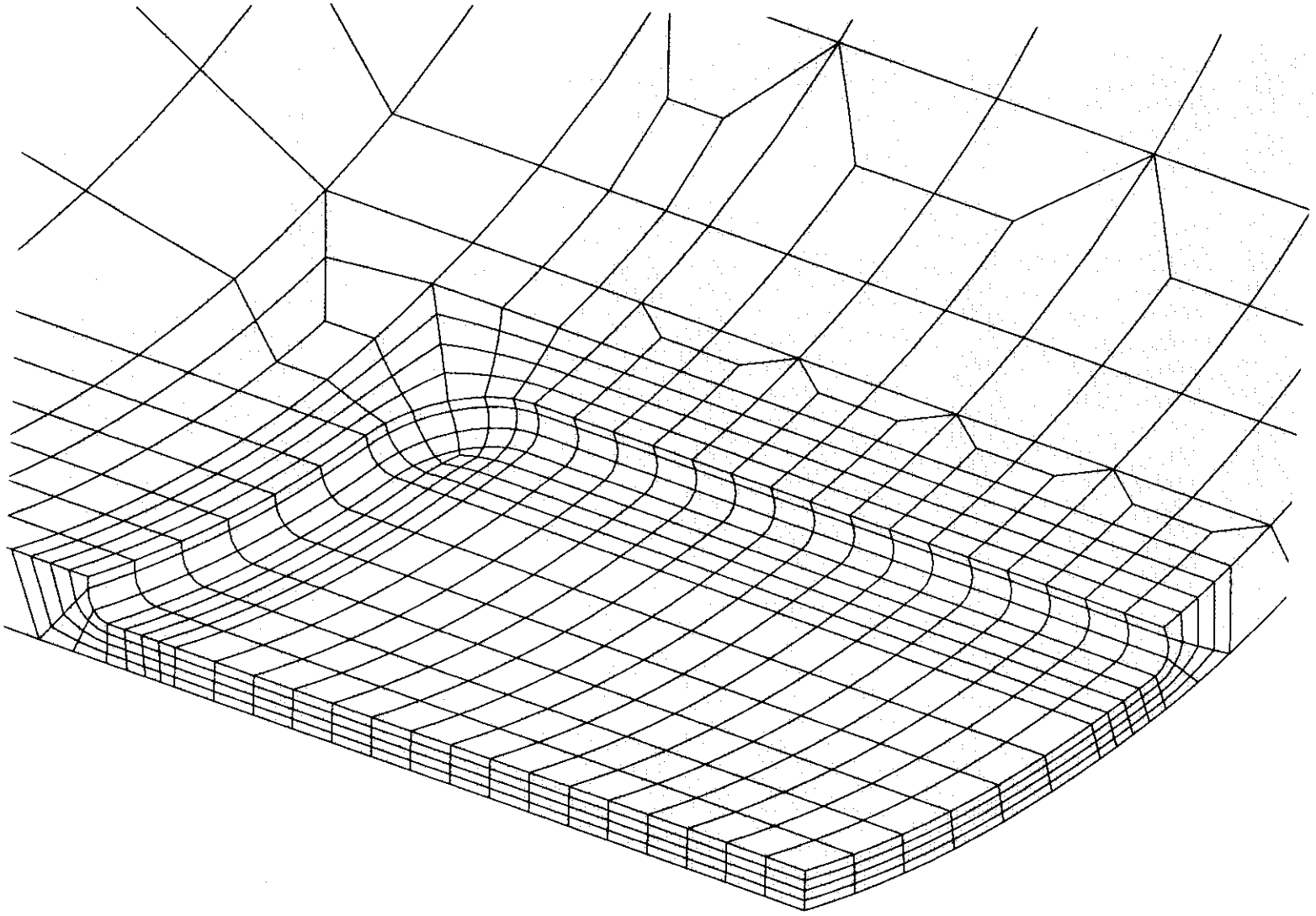

Figure 3-10 Example of typical finite element model, close-up view. D = 324 mm, t = 10.0 mm, d/t= 0.5, L/D = 0.75, w=15t

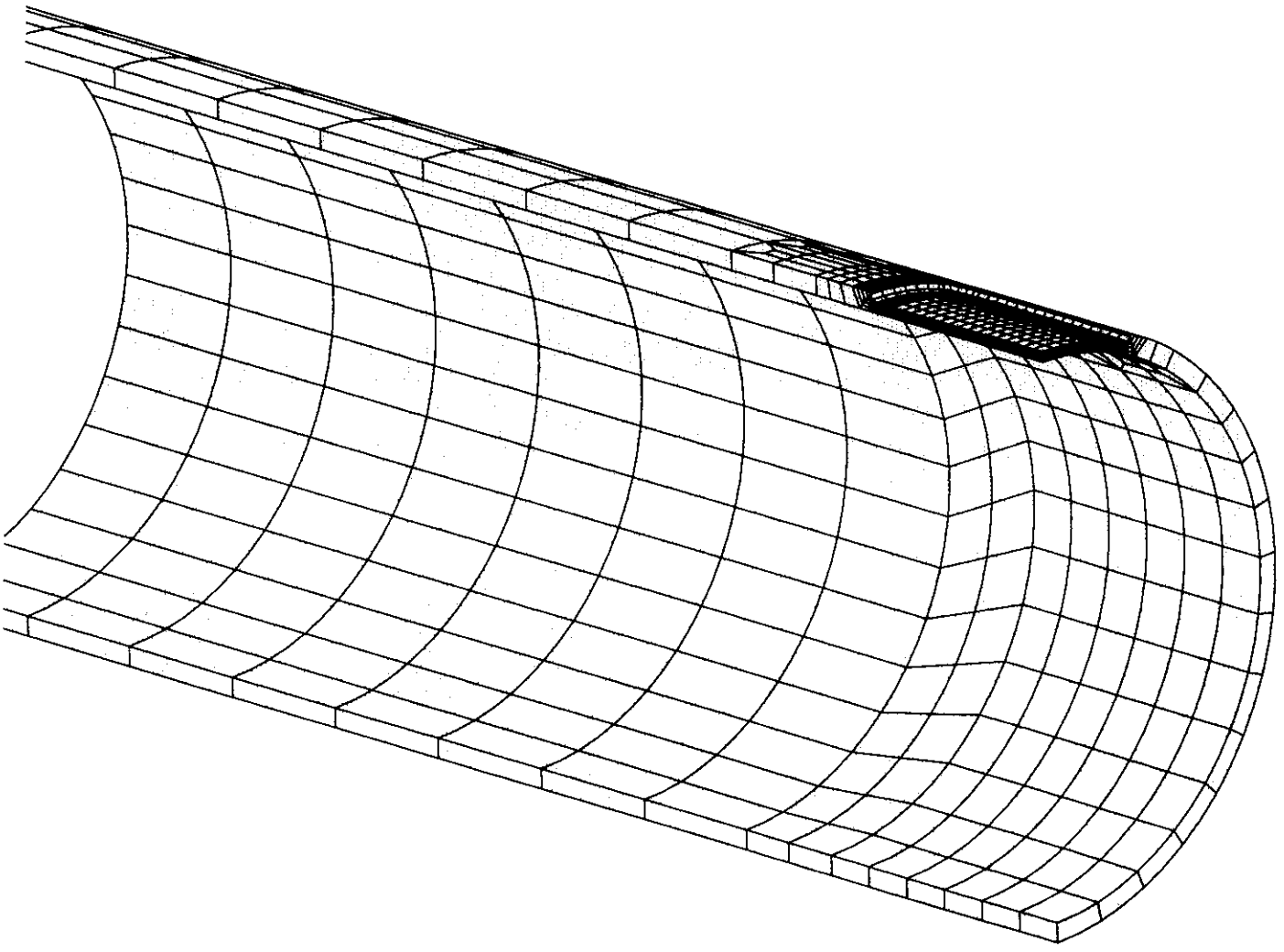

Figure 3-11 Example of typical finite element model, general view. D = 324 mm, t = 10.0 mm, d/t= 0.5, L/D = 0.75, w=15t, outside corrosion defect

4 LONGITUDINAL CORROSION DEFECTS, INTERNAL PRESSURE

4.1 3D analyses

4.1.1 Corrosion depth and length sensitivity

A series of analyses were performed with internal pressure with smooth rectangular shaped corrosion defects with various length and depth, and both the X60 and the X80 material were used. The results are shown in Figure 4-1 for the analyses with X60 material, and in Figure 4-2 for the analyses with X80 material. The capacity equation developed within this project is based upon these results for the corrosion defect length and depth parameters. The results are normalised to P_0, which is defined as

$$P_0 = \frac{2 \cdot t}{D - t} \cdot \sigma_u \qquad (4.1)$$

σ_u : ultimate tensile strength
t : pipe wall thickness
D : pipe outer diameter

The results are given in tabular form in the next pages.

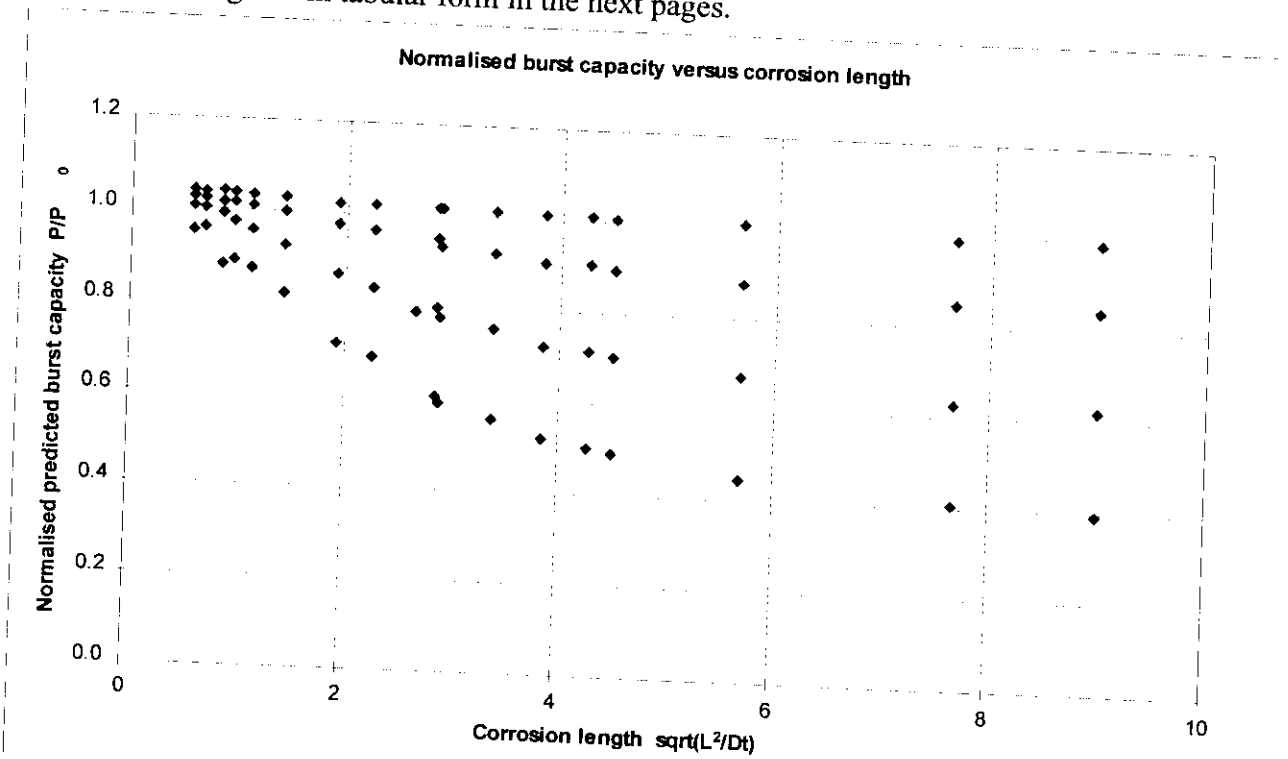

Figure 4-1 Normalised burst capacity, X60 material

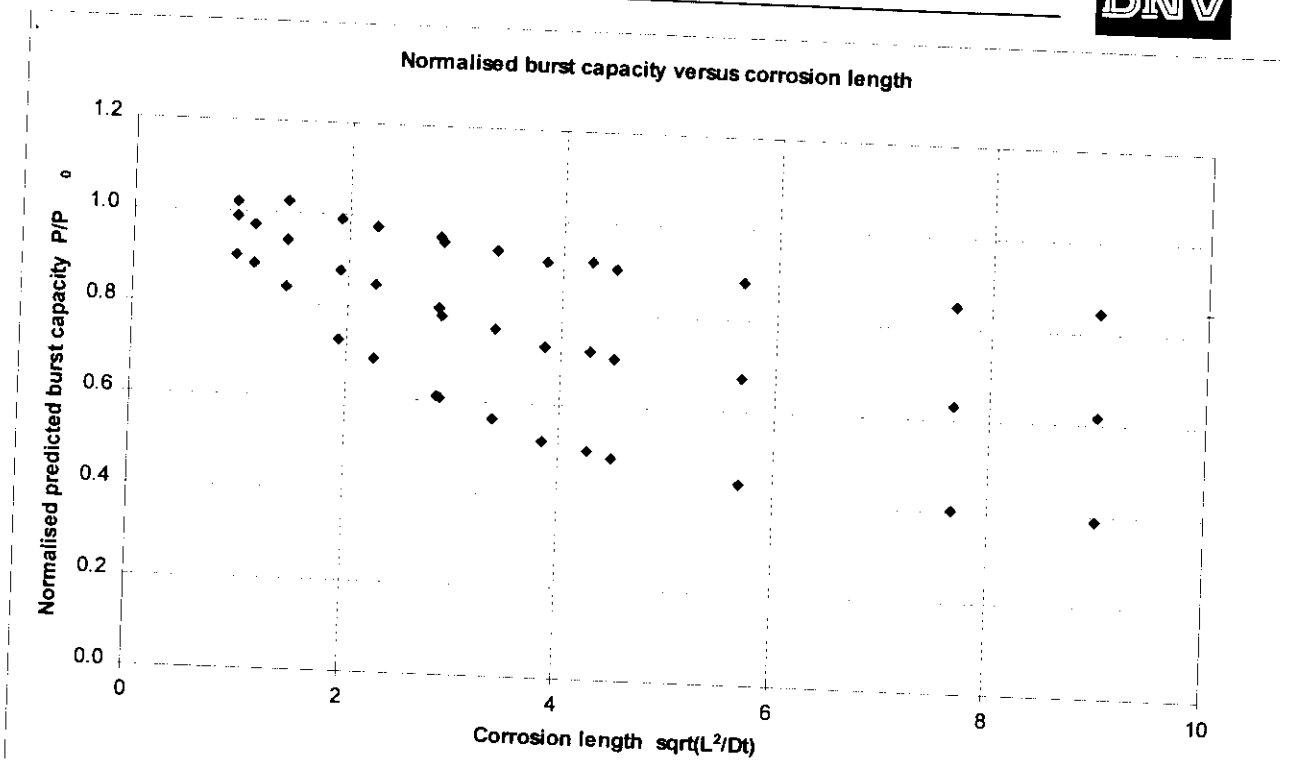

Figure 4-2 Normalised burst capacity, X80 material

LONGITUDINAL CORROSION DEFECTS, INTERNAL PRESSURE

ID	mm Dia	mm t	mm L	mm d	w/t	Dia/t	L/Dia	d/t	sqrt(L2/(Di	Shape	MPa Yield	MPa UTS	Material	bar P0	bar PC	PC/P0
DNV-S43	324	10	48.6	1.5	3	32.4	0.15	15 %	0.85	rect.	460	578	X60mm	368.2	383	1.040
DNV-S44	324	10	81.0	1.5	3	32.4	0.25	15 %	1.42	rect.	460	578	X60mm	368.2	380	1.032
DNV-S45	324	10	162.0	1.5	3	32.4	0.5	15 %	2.85	rect.	460	578	X60mm	368.2	375	1.019
DNV-S46	324	10	243.0	1.5	3	32.4	0.75	15 %	4.27	rect.	460	578	X60mm	368.2	372	1.010
DNV-S47	324	10	324.0	1.5	3	32.4	1	15 %	5.69	rect.	460	578	X60mm	368.2	370	1.005
DNV-S48	324	10	648.0	1.5	3	32.4	2.	15 %	11.38	rect.	460	578	X60mm	368.2	364.6	0.990
DNV-P1	324	10	1500.0	1.5	3	32.4	4.63	15 %	26.35	rect.	460	578	X60mm	368.2	363.4	0.987
DNV-S16	324	10	48.6	3	3	32.4	0.15	30 %	0.85	rect.	460	578	X60mm	368.2	374	1.016
DNV-S17	324	10	81.0	3	3	32.4	0.25	30 %	1.42	rect.	460	578	X60mm	368.2	368	1.000
DNV-S18	324	10	162.0	3	3	32.4	0.5	30 %	2.85	rect.	460	578	X60mm	368.2	350	0.951
DNV-S19	324	10	243.0	3	3	32.4	0.75	30 %	4.27	rect.	460	578	X60mm	368.2	333	0.905
DNV-S20	324	10	324.0	3	3	32.4	1	30 %	5.69	rect.	460	578	X60mm	368.2	323.2	0.878
DNV-S34	324	10	648.0	3	3	32.4	2.	30 %	11.38	rect.	460	578	X60mm	368.2	305.5	0.830
DNV-P2	324	10	1500.0	3	3	32.4	4.63	30 %	26.35	rect.	460	578	X60mm	368.2	302.8	0.822
DNV-S21	324	10	48.6	5	3	32.4	0.15	50 %	0.85	rect.	460	578	X60mm	368.2	365	0.991
DNV-S22	324	10	81.0	5	3	32.4	0.25	50 %	1.42	rect.	460	578	X60mm	368.2	340.7	0.925
DNV-S23	324	10	162.0	5	3	32.4	0.5	50 %	2.85	rect.	460	578	X60mm	368.2	293.6	0.797
DNV-S24	324	10	243.0	5	3	32.4	0.75	50 %	4.27	rect.	460	578	X60mm	368.2	263.4	0.715
DNV-S25	324	10	324.0	5	3	32.4	1	50 %	5.69	rect.	460	578	X60mm	368.2	247.7	0.673
DNV-S35	324	10	648.0	5	3	32.4	2.	50 %	11.38	rect.	460	578	X60mm	368.2	223.5	0.607
DNV-P3	324	10	1500.0	5	3	32.4	4.63	50 %	26.35	rect.	460	578	X60mm	368.2	216.5	0.588
DNV-S26	324	10	48.6	7	3	32.4	0.15	70 %	0.85	rect.	460	578	X60mm	368.2	324	0.880
DNV-S27	324	10	81.0	7	3	32.4	0.25	70 %	1.42	rect.	460	578	X60mm	368.2	301.8	0.820
DNV-S28	324	10	162.0	7	3	32.4	0.5	70 %	2.85	rect.	460	578	X60mm	368.2	223.3	0.607
DNV-S29	324	10	243.0	7	3	32.4	0.75	70 %	4.27	rect.	460	578	X60mm	368.2	185.2	0.503
DNV-S30	324	10	324.0	7	3	32.4	1	70 %	5.69	rect.	460	578	X60mm	368.2	164.8	0.448
DNV-S36	324	10	648.0	7	3	32.4	2.	70 %	11.38	rect.	460	578	X60mm	368.2	137.6	0.374
DNV-P4	324	10	1500.0	7	3	32.4	4.63	70 %	26.35	rect.	460	578	X60mm	368.2	129.8	0.353
DNV-S37	324	16	48.6	2.4	3	20.25	0.15	15 %	0.68	rect.	460	578	X60mm	600.5	623	1.037
DNV-S38	324	16	81.0	2.4	3	20.25	0.25	15 %	1.13	rect.	460	578	X60mm	600.5	621	1.034
DNV-S39	324	16	162.0	2.4	3	20.25	0.5	15 %	2.25	rect.	460	578	X60mm	600.5	612	1.019
DNV-S40	324	16	243.0	2.4	3	20.25	0.75	15 %	3.38	rect.	460	578	X60mm	600.5	608	1.012
DNV-S41	324	16	324.0	2.4	3	20.25	1	15 %	4.50	rect.	460	578	X60mm	600.5	604.1	1.006
DNV-S42	324	16	648.0	2.4	3	20.25	2.	15 %	9.00	rect.	460	578	X60mm	600.5	594.5	0.990
DNV-P6	324	16	1500.0	2.4	3	20.25	4.63	15 %	20.83	rect.	460	578	X60mm	600.5	591.2	0.984
DNV-S1	324	16	48.6	4.8	3	20.25	0.15	30 %	0.68	rect.	460	578	X60mm	600.5	616	1.026
DNV-S2	324	16	81.0	4.8	3	20.25	0.25	30 %	1.13	rect.	460	578	X60mm	600.5	606	1.009
DNV-S3	324	16	162.0	4.8	3	20.25	0.5	30 %	2.25	rect.	460	578	X60mm	600.5	578	0.963
DNV-S4	324	16	243.0	4.8	3	20.25	0.75	30 %	3.38	rect.	460	578	X60mm	600.5	553.7	0.922
DNV-S5	324	16	324.0	4.8	3	20.25	1	30 %	4.50	rect.	460	578	X60mm	600.5	537.1	0.894
DNV-S32	324	16	648.0	4.8	3	20.25	2.	30 %	9.00	rect.	460	578	X60mm	600.5	505.7	0.842
DNV-P7	324	16	1500.0	4.8	3	20.25	4.63	30 %	20.83	rect.	460	578	X60mm	600.5	492.6	0.820
DNV-S6	324	16	48.6	8	3	20.25	0.15	50 %	0.68	rect.	460	578	X60mm	600.5	602	1.002
DNV-S7	324	16	81.0	8	3	20.25	0.25	50 %	1.13	rect.	460	578	X60mm	600.5	575.1	0.958
DNV-S8	324	16	162.0	8	3	20.25	0.5	50 %	2.25	rect.	460	578	X60mm	600.5	503.5	0.838
DNV-S9	324	16	243.0	8	3	20.25	0.75	50 %	3.38	rect.	460	578	X60mm	600.5	454.2	0.756
DNV-S10	324	16	324.0	8	3	20.25	1	50 %	4.50	rect.	460	578	X60mm	600.5	423	0.704
DNV-S32_2	324	16	648.0	8	3	20.25	2.	50 %	9.00	rect.	460	578	X60mm	600.5	373	0.621
DNV-P8	324	16	1500.0	8	3	20.25	4.63	50 %	20.83	rect.	460	578	X60mm	600.5	352	0.586
DNV-S75	324	16	190.5	8.0	3	20.25	0.588	50 %	2.65	rect.	460	578	X60mm	600.5	474	0.789
DNV-S11	324	16	48.6	11.2	3	20.25	0.15	70 %	0.68	rect.	460	578	X60mm	600.5	576	0.959
DNV-S12	324	16	81.0	11.2	3	20.25	0.25	70 %	1.13	rect.	460	578	X60mm	600.5	524.3	0.873
DNV-S13	324	16	162.0	11.2	3	20.25	0.5	70 %	2.25	rect.	460	578	X60mm	600.5	411.6	0.685
DNV-S14	324	16	243.0	11.2	3	20.25	0.75	70 %	3.38	rect.	460	578	X60mm	600.5	336.8	0.561
DNV-S15	324	16	324.0	11.2	3	20.25	1	70 %	4.50	rect.	460	578	X60mm	600.5	295.6	0.492
DNV-S33	324	16	648.0	11.2	3	20.25	2.	70 %	9.00	rect.	460	578	X60mm	600.5	235.7	0.392
DNV-P9	324	16	1500.0	11.2	3	20.25	4.63	70 %	20.83	rect.	460	578	X60mm	600.5	211	0.351
	324	22	48.6	3.3	3	14.727	0.15	15 %	0.58	rect.	460	578	X60mm	842.1	877	1.041
DNV-S50	324	22	81.0	3.3	3	14.727	0.25	15 %	0.96	rect.	460	578	X60mm	842.1	875	1.039
DNV-S51	324	22	162.0	3.3	3	14.727	0.5	15 %	1.92	rect.	460	578	X60mm	842.1	860	1.021
DNV-S52	324	22	243.0	3.3	3	14.727	0.75	15 %	2.88	rect.	460	578	X60mm	842.1	855	1.015
DNV-S53	324	22	324.0	3.3	3	14.727	1	15 %	3.84	rect.	460	578	X60mm	842.1	850	1.009
DNV-S54	324	22	648.0	3.3	3	14.727	2.	15 %	7.68	rect.	460	578	X60mm	842.1	833.9	0.990
DNV-P11	324	22	1500.0	3.3	3	14.727	4.63	15 %	17.77	rect.	460	578	X60mm	842.1	827.2	0.982
	324	22	48.6	6.6	3	14.727	0.15	30 %	0.58	rect.	460	578	X60mm	842.1	864	1.026
DNV-S56	324	22	81.0	6.6	3	14.727	0.25	30 %	0.96	rect.	460	578	X60mm	842.1	856	1.016
DNV-S57	324	22	162.0	6.6	3	14.727	0.5	30 %	1.92	rect.	460	578	X60mm	842.1	821.4	0.975

ID	mm Dia	mm t	mm L	mm d	w/t	Dia/t	L/Dia	d/t	sqrt(L2/(Di	Shape	MPa Yield	MPa UTS	Material	bar P0	bar PC	PC/P0
DNV-S101	324	10	81.0	3	3	32.4	0.25	30 %	1.42	rect.	601	727	X80mm	463.1	474	1.024
DNV-S102	324	10	162.0	3	3	32.4	0.5	30 %	2.85	rect.	601	727	X80mm	463.1	443.5	0.958
DNV-S103	324	10	243.0	3	3	32.4	0.75	30 %	4.27	rect.	601	727	X80mm	463.1	423.5	0.915
DNV-S104	324	10	324.0	3	3	32.4	1	30 %	5.69	rect.	601	727	X80mm	463.1	409.8	0.885
DNV-S105	324	10	648.0	3	3	32.4	2.	30 %	11.38	rect.	601	727	X80mm	463.1	386.3	0.834
DNV-S91	324	10	81.0	5	3	32.4	0.25	50 %	1.42	rect.	601	727	X80mm	463.1	435.9	0.941
DNV-S92	324	10	162.0	5	3	32.4	0.5	50 %	2.85	rect.	601	727	X80mm	463.1	372.6	0.805
DNV-S93	324	10	243.0	5	3	32.4	0.75	50 %	4.27	rect.	601	727	X80mm	463.1	333.8	0.721
DNV-S94	324	10	324.0	5	3	32.4	1	50 %	5.69	rect.	601	727	X80mm	463.1	312.2	0.674
DNV-S95	324	10	648.0	5	3	32.4	2.	50 %	11.38	rect.	601	727	X80mm	463.1	280.7	0.606
DNV-S96	324	10	81.0	7	3	32.4	0.25	70 %	1.42	rect.	601	727	X80mm	463.1	388	0.838
DNV-S97	324	10	162.0	7	3	32.4	0.5	70 %	2.85	rect.	601	727	X80mm	463.1	282.3	0.610
DNV-S98	324	10	243.0	7	3	32.4	0.75	70 %	4.27	rect.	601	727	X80mm	463.1	231.6	0.500
DNV-S99	324	10	324.0	7	3	32.4	1	70 %	5.69	rect.	601	727	X80mm	463.1	205.3	0.443
DNV-S100	324	10	648.0	7	3	32.4	2.	70 %	11.38	rect.	601	727	X80mm	463.1	171.9	0.371
DNV-S107	324	16	162.0	4.8	3	20.25	0.5	30 %	2.25	rect.	601	727	X80mm	755.3	737.9	0.977
DNV-S108	324	16	243.0	4.8	3	20.25	0.75	30 %	3.38	rect.	601	727	X80mm	755.3	705.1	0.934
DNV-S109	324	16	324.0	4.8	3	20.25	1	30 %	4.50	rect.	601	727	X80mm	755.3	681.3	0.902
DNV-S110	324	16	648.0	4.8	3	20.25	2.	30 %	9.00	rect.	601	727	X80mm	755.3	637.4	0.844
DNV-S111	324	16	81.0	8	3	20.25	0.25	50 %	1.13	rect.	601	727	X80mm	755.3	735.4	0.974
DNV-S112	324	16	162.0	8	3	20.25	0.5	50 %	2.25	rect.	601	727	X80mm	755.3	640.9	0.849
DNV-S113	324	16	243.0	8	3	20.25	0.75	50 %	3.38	rect.	601	727	X80mm	755.3	574.5	0.761
DNV-S114	324	16	324.0	8	3	20.25	1	50 %	4.50	rect.	601	727	X80mm	755.3	532.7	0.705
DNV-S115	324	16	648.0	8	3	20.25	2.	50 %	9.00	rect.	601	727	X80mm	755.3	467.4	0.619
DNV-S116	324	16	81.0	11.2	3	20.25	0.25	70 %	1.13	rect.	601	727	X80mm	755.3	670.9	0.888
DNV-S117	324	16	162.0	11.2	3	20.25	0.5	70 %	2.25	rect.	601	727	X80mm	755.3	520	0.688
DNV-S118	324	16	243.0	11.2	3	20.25	0.75	70 %	3.38	rect.	601	727	X80mm	755.3	427.5	0.566
DNV-S119	324	16	324.0	11.2	3	20.25	1	70 %	4.50	rect.	601	727	X80mm	755.3	369.1	0.489
DNV-S120	324	16	648.0	11.2	3	20.25	2.	70 %	9.00	rect.	601	727	X80mm	755.3	293.2	0.388
DNV-S86	324	22	81.0	6.6	3	14.727	0.25	30 %	0.96	rect.	601	727	X80mm	1059.2	1080	1.020
DNV-S87	324	22	162.0	6.6	3	14.727	0.5	30 %	1.92	rect.	601	727	X80mm	1059.2	1048.4	0.990
DNV-S88	324	22	243.0	6.6	3	14.727	0.75	30 %	2.88	rect.	601	727	X80mm	1059.2	1002.2	0.946
DNV-S89	324	22	324.0	6.6	3	14.727	1	30 %	3.84	rect.	601	727	X80mm	1059.2	968.1	0.914
DNV-S90	324	22	648.0	6.6	3	14.727	2.	30 %	7.68	rect.	601	727	X80mm	1059.2	901	0.851
DNV-S76	324	22	81.0	11	3	14.727	0.25	50 %	0.96	rect.	601	727	X80mm	1059.2	1047.6	0.989
DNV-S77	324	22	162.0	11	3	14.727	0.5	50 %	1.92	rect.	601	727	X80mm	1059.2	928.2	0.876
DNV-S78	324	22	243.0	11	3	14.727	0.75	50 %	2.88	rect.	601	727	X80mm	1059.2	832.8	0.786
DNV-S79	324	22	324.0	11	3	14.727	1	50 %	3.84	rect.	601	727	X80mm	1059.2	770.9	0.728
DNV-S80	324	22	648.0	11	3	14.727	2.	50 %	7.68	rect.	601	727	X80mm	1059.2	667.9	0.631
DNV-S81	324	22	81.0	15.4	3	14.727	0.25	70 %	0.96	rect.	601	727	X80mm	1059.2	960.3	0.907
DNV-S82	324	22	162.0	15.4	3	14.727	0.5	70 %	1.92	rect.	601	727	X80mm	1059.2	769.7	0.727
DNV-S83	324	22	243.0	15.4	3	14.727	0.75	70 %	2.88	rect.	601	727	X80mm	1059.2	643	0.607
DNV-S84	324	22	324.0	15.4	3	14.727	1	70 %	3.84	rect.	601	727	X80mm	1059.2	550.4	0.520
DNV-S85	324	22	648.0	15.4	3	14.727	2.	70 %	7.68	rect.	601	727	X80mm	1059.2	427.2	0.403

4.1.2 Material sensitivity, variations of the average X60 material

A few models were selected for a study of the sensitivity to variations of the material. The material yield strength and tensile strength were varied with ±10% which resulted in 3 levels of yield strength and 3 levels of tensile strength, a total of 9 combinations, see section 3.8. Some of the combination can seem odd and may not be a realistic material, but it is considered to be appropriate for the sensitivity study. The analysis id and the material label include 2 letters, where the first indicate the yield stress and the second one indicate the ultimate stress, where m is "mean" u is "upper 10%, and l is lower 10%.

The results of the analyses are shown in Figure 4-3 and in Table 4-1. The results grouped together are calculated burst capacities for combinations of the material using the same FE geometry model.

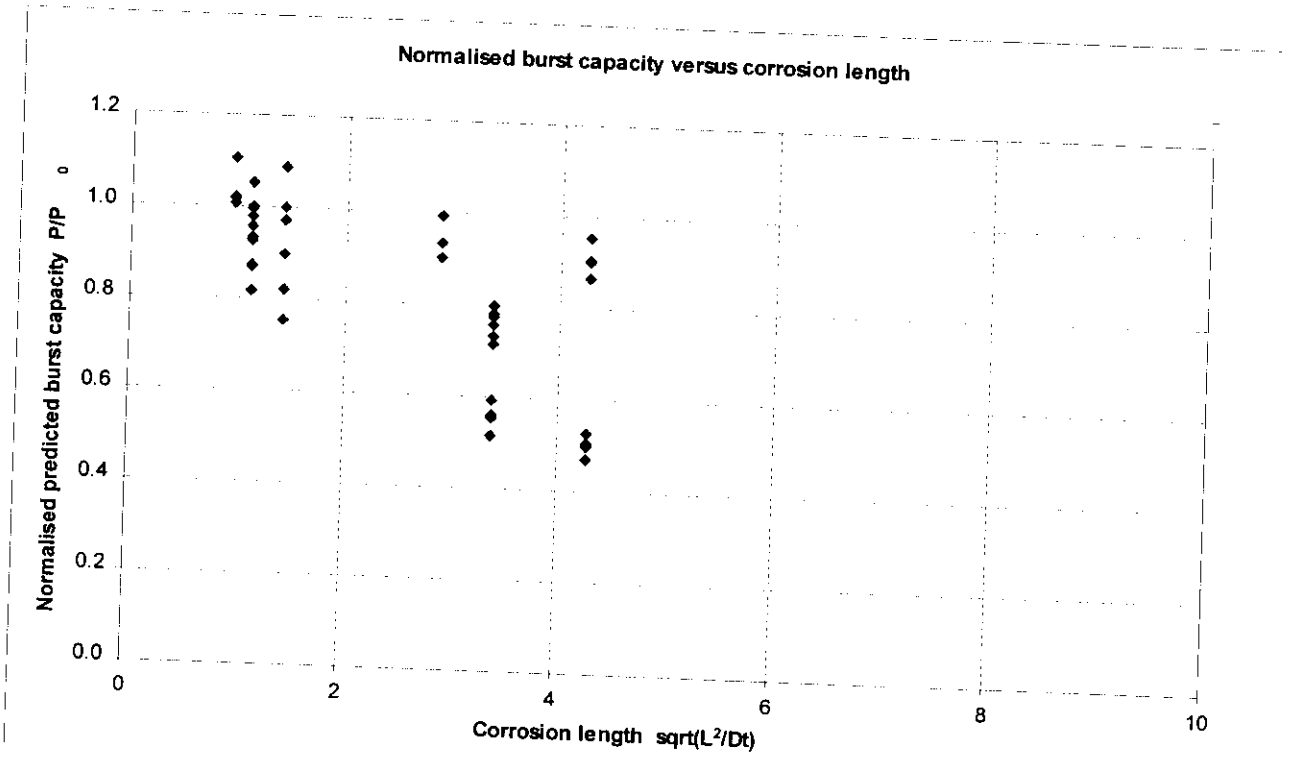

Figure 4-3 Results of the material sensitivity study

Table 4-1 Results of the material sensitivity study

ID	mm Dia	mm t	mm L	mm d	w/t	Dia/t	L/Dia	d/t	sqrt(L2/(Di	Shape	MPa Yield	MPa UTS	Material	bar P0	bar PC	PC/P0
DNV-S17	324	10	81.0	3	3	32.4	0.25	30 %	1.42	rect.	460	578	X60mm	368.2	368	1.000
DNV-S17uu	324	10	81.0	3	3	32.4	0.25	30 %	1.42	rect.	506	636	X60uu	405.1	405	1.000
DNV-S17ul	324	10	81.0	3	3	32.4	0.25	30 %	1.42	rect.	506	520	X60ul	331.2	360.6	1.089
DNV-S17lu	324	10	81.0	3	3	32.4	0.25	30 %	1.42	rect.	414	636	X60lu	405.1	393.1	0.970
DNV-S17ll	324	10	81.0	3	3	32.4	0.25	30 %	1.42	rect.	414	520	X60ll	331.2	331	0.999
DNV-S19	324	10	243.0	3	3	32.4	0.75	30 %	4.27	rect.	460	578	X60mm	368.2	333	0.905
DNV-S19uu	324	10	243.0	3	3	32.4	0.75	30 %	4.27	rect.	506	636	X60uu	405.1	365.4	0.902
DNV-S19ul	324	10	243.0	3	3	32.4	0.75	30 %	4.27	rect.	506	520	X60ul	331.2	316.3	0.955
DNV-S19lu	324	10	243.0	3	3	32.4	0.75	30 %	4.27	rect.	414	636	X60lu	405.1	350.9	0.866
DNV-S19ll	324	10	243.0	3	3	32.4	0.75	30 %	4.27	rect.	414	520	X60ll	331.2	299.3	0.904
DNV-S27	324	10	81.0	7	3	32.4	0.25	70 %	1.42	rect.	460	578	X60mm	368.2	301.8	0.820
DNV-S27uu	324	10	81.0	7	3	32.4	0.25	70 %	1.42	rect.	506	636	X60uu	405.1	331.9	0.819
DNV-S27ul	324	10	81.0	7	3	32.4	0.25	70 %	1.42	rect.	506	520	X60ul	331.2	297.2	0.897
DNV-S27lu	324	10	81.0	7	3	32.4	0.25	70 %	1.42	rect.	414	636	X60lu	405.1	305	0.753
DNV-S27ll	324	10	81.0	7	3	32.4	0.25	70 %	1.42	rect.	414	520	X60ll	331.2	271.6	0.820
DNV-S29	324	10	243.0	7	3	32.4	0.75	70 %	4.27	rect.	460	578	X60mm	368.2	185.2	0.503
DNV-S29uu	324	10	243.0	7	3	32.4	0.75	70 %	4.27	rect.	506	636	X60uu	405.1	202	0.499
DNV-S29ul	324	10	243.0	7	3	32.4	0.75	70 %	4.27	rect.	506	520	X60ul	331.2	174.7	0.527
DNV-S29lu	324	10	243.0	7	3	32.4	0.75	70 %	4.27	rect.	414	636	X60lu	405.1	191	0.471
DNV-S29ll	324	10	243.0	7	3	32.4	0.75	70 %	4.27	rect.	414	520	X60ll	331.2	166.9	0.504
DNV-S7	324	16	81.0	8	3	20.25	0.25	50 %	1.13	rect.	460	578	X60mm	600.5	575.1	0.958
DNV-S7mu	324	16	81.0	8	3	20.25	0.25	50 %	1.13	rect.	460	636	X60mu	660.8	615.1	0.931
DNV-S7ml	324	16	81.0	8	3	20.25	0.25	50 %	1.13	rect.	460	520	X60ml	540.3	540.1	1.000
DNV-S7um	324	16	81.0	8	3	20.25	0.25	50 %	1.13	rect.	506	578	X60um	600.5	597.5	0.995
DNV-S7uu	324	16	81.0	8	3	20.25	0.25	50 %	1.13	rect.	506	636	X60uu	660.8	611	0.925
DNV-S7ul	324	16	81.0	8	3	20.25	0.25	50 %	1.13	rect.	506	520	X60ul	540.3	569	1.053
DNV-S7lm	324	16	81.0	8	3	20.25	0.25	50 %	1.13	rect.	414	578	X60lm	600.5	560	0.933
DNV-S7lu	324	16	81.0	8	3	20.25	0.25	50 %	1.13	rect.	414	636	X60lu	660.8	575	0.870
DNV-S7ll	324	16	81.0	8	3	20.25	0.25	50 %	1.13	rect.	414	520	X60ll	540.3	529	0.979
DNV-S9	324	16	243.0	8	3	20.25	0.75	50 %	3.38	rect.	460	578	X60mm	600.5	454.2	0.756
DNV-S9mu	324	16	243.0	8	3	20.25	0.75	50 %	3.38	rect.	460	636	X60mu	660.8	485.6	0.735
DNV-S9ml	324	16	243.0	8	3	20.25	0.75	50 %	3.38	rect.	460	520	X60ml	540.3	422.1	0.781
DNV-S9um	324	16	243.0	8	3	20.25	0.75	50 %	3.38	rect.	506	578	X60um	600.5	466.4	0.777
DNV-S9uu	324	16	243.0	8	3	20.25	0.75	50 %	3.38	rect.	506	636	X60uu	660.8	499.9	0.757
DNV-S9ul	324	16	243.0	8	3	20.25	0.75	50 %	3.38	rect.	506	520	X60ul	540.3	432.1	0.800
DNV-S9lm	324	16	243.0	8	3	20.25	0.75	50 %	3.38	rect.	414	578	X60lm	600.5	440	0.733
DNV-S9lu	324	16	243.0	8	3	20.25	0.75	50 %	3.38	rect.	414	636	X60lu	660.8	472.5	0.715
DNV-S9ll	324	16	243.0	8	3	20.25	0.75	50 %	3.38	rect.	414	520	X60ll	540.3	409.3	0.758
DNV-S12	324	16	81.0	11.2	3	20.25	0.25	70 %	1.13	rect.	460	578	X60mm	600.5	524.3	0.873
DNV-S12uu	324	16	81.0	11.2	3	20.25	0.25	70 %	1.13	rect.	506	636	X60uu	660.8	576.5	0.872
DNV-S12ul	324	16	81.0	11.2	3	20.25	0.25	70 %	1.13	rect.	506	520	X60ul	540.3	517	0.957
DNV-S12lu	324	16	81.0	11.2	3	20.25	0.25	70 %	1.13	rect.	414	636	X60lu	660.8	539.4	0.816
DNV-S12ll	324	16	81.0	11.2	3	20.25	0.25	70 %	1.13	rect.	414	520	X60ll	540.3	471.1	0.872
DNV-S14	324	16	243.0	11.2	3	20.25	0.75	70 %	3.38	rect.	460	578	X60mm	600.5	336.8	0.561
DNV-S14uu	324	16	243.0	11.2	3	20.25	0.75	70 %	3.38	rect.	506	636	X60uu	660.8	366.3	0.554
DNV-S14ul	324	16	243.0	11.2	3	20.25	0.75	70 %	3.38	rect.	506	520	X60ul	540.3	320.2	0.593
DNV-S14lu	324	16	243.0	11.2	3	20.25	0.75	70 %	3.38	rect.	414	636	X60lu	660.8	341.5	0.517
DNV-S14ll	324	16	243.0	11.2	3	20.25	0.75	70 %	3.38	rect.	414	520	X60ll	540.3	301.2	0.558
DNV-S56	324	22	81.0	6.6	3	14.727	0.25	30 %	0.96	rect.	460	578	X60mm	842.1	856	1.016
DNV-S56uu	324	22	81.0	6.6	3	14.727	0.25	30 %	0.96	rect.	506	636	X60uu	926.6	945	1.020
DNV-S56ul	324	22	81.0	6.6	3	14.727	0.25	30 %	0.96	rect.	506	520	X60ul	757.6	836.2	1.104
DNV-S56lu	324	22	81.0	6.6	3	14.727	0.25	30 %	0.96	rect.	414	636	X60lu	926.6	932.1	1.006
DNV-S56ll	324	22	81.0	6.6	3	14.727	0.25	30 %	0.96	rect.	414	520	X60ll	757.6	772	1.019
DNV-S58	324	22	243.0	6.6	3	14.727	0.75	30 %	2.88	rect.	460	578	X60mm	842.1	786.5	0.934
DNV-S58uu	324	22	243.0	6.6	3	14.727	0.75	30 %	2.88	rect.	506	636	X60uu	926.6	866	0.935
DNV-S58ul	324	22	243.0	6.6	3	14.727	0.75	30 %	2.88	rect.	506	520	X60ul	757.6	753.6	0.995
DNV-S58lu	324	22	243.0	6.6	3	14.727	0.75	30 %	2.88	rect.	414	636	X60lu	926.6	834.7	0.901
DNV-S58ll	324	22	243.0	6.6	3	14.727	0.75	30 %	2.88	rect.	414	520	X60ll	757.6	707.2	0.933

4.1.3 Parabolic shaped corrosion defect

A few models with parabolic shaped corrosion defect were generated, and analysed with internal pressure loading. The result shows an increase in burst capacity, see Figure 4-4. The upper line is the results for the 4 models with parabolic shaped corrosion defect, and the corresponding analyses with rectangular shaped corrosion defect are shown in the lower line. An example of the models is shown in Figure 4-5. An attempt was made to generate a number of models with parabolic shaped corrosion defect in a simple manner using one basic model and change the co-ordinates by use of a small software routine. Nice looking shaped corrosion defects were generated, but the elements at the edges of the corrosion defects did not show convincing behaviour, and hence the results from the analyses are not included in the report.

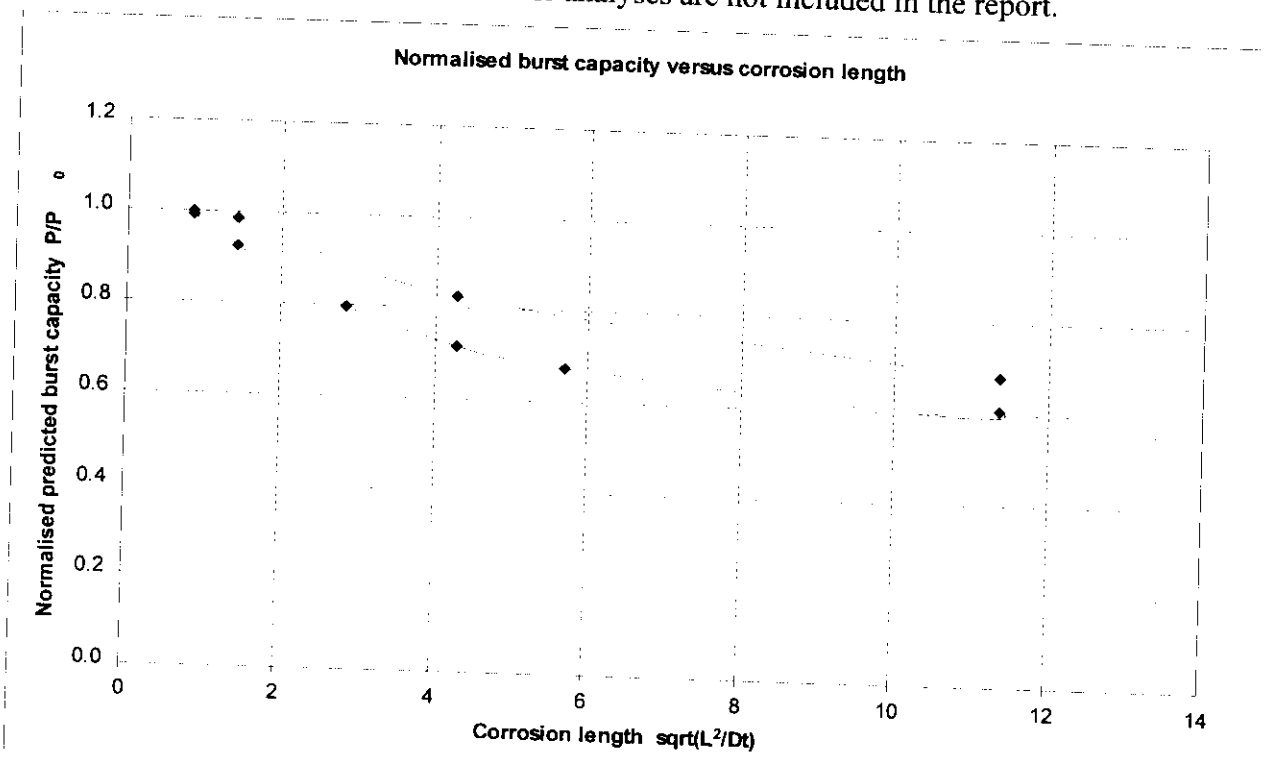

Figure 4-4 Parabolic shaped corrosion (parabolic upper line, rectangular lower line)

Table 4-2 Results for the analyses with parabolic shaped corrosion (4 last rows)

ID	mm Dia	mm t	mm L	mm d	w/t	Dia/t	L/Dia	d/t	sqrt(L2/(Di	Shape	MPa Yield	MPa UTS	Material	bar P0	bar PC	PC/P0
DNV-S21	324	10	48.6	5	3	32.4	0.15	50 %	0.85	rect.	460	578	X60mm	368.2	365	0.991
DNV-S22	324	10	81.0	5	3	32.4	0.25	50 %	1.42	rect.	460	578	X60mm	368.2	340.7	0.925
DNV-S23	324	10	162.0	5	3	32.4	0.5	50 %	2.85	rect.	460	578	X60mm	368.2	293.6	0.797
DNV-S24	324	10	243.0	5	3	32.4	0.75	50 %	4.27	rect.	460	578	X60mm	368.2	263.4	0.715
DNV-S25	324	10	324.0	5	3	32.4	1	50 %	5.69	rect.	460	578	X60mm	368.2	247.7	0.673
DNV-S35	324	10	648.0	5	3	32.4	2	50 %	11.38	rect.	460	578	X60mm	368.2	223.5	0.607
DNV-rec10	324	10	48.6	5	3	32.4	0.15	50 %	0.85	parabel	460	578	X60mm	368.2	368	1.000
DNV-rec10	324	10	81.0	5	3	32.4	0.25	50 %	1.42	parabel	460	578	X60mm	368.2	362.5	0.985
DNV-rec10	324	10	243.0	5	3	32.4	0.75	50 %	4.27	parabel	460	578	X60mm	368.2	304	0.826
DNV-rec10	324	10	648.0	5	3	32.4	2	50 %	11.38	parabel	460	578	X60mm	368.2	251	0.682

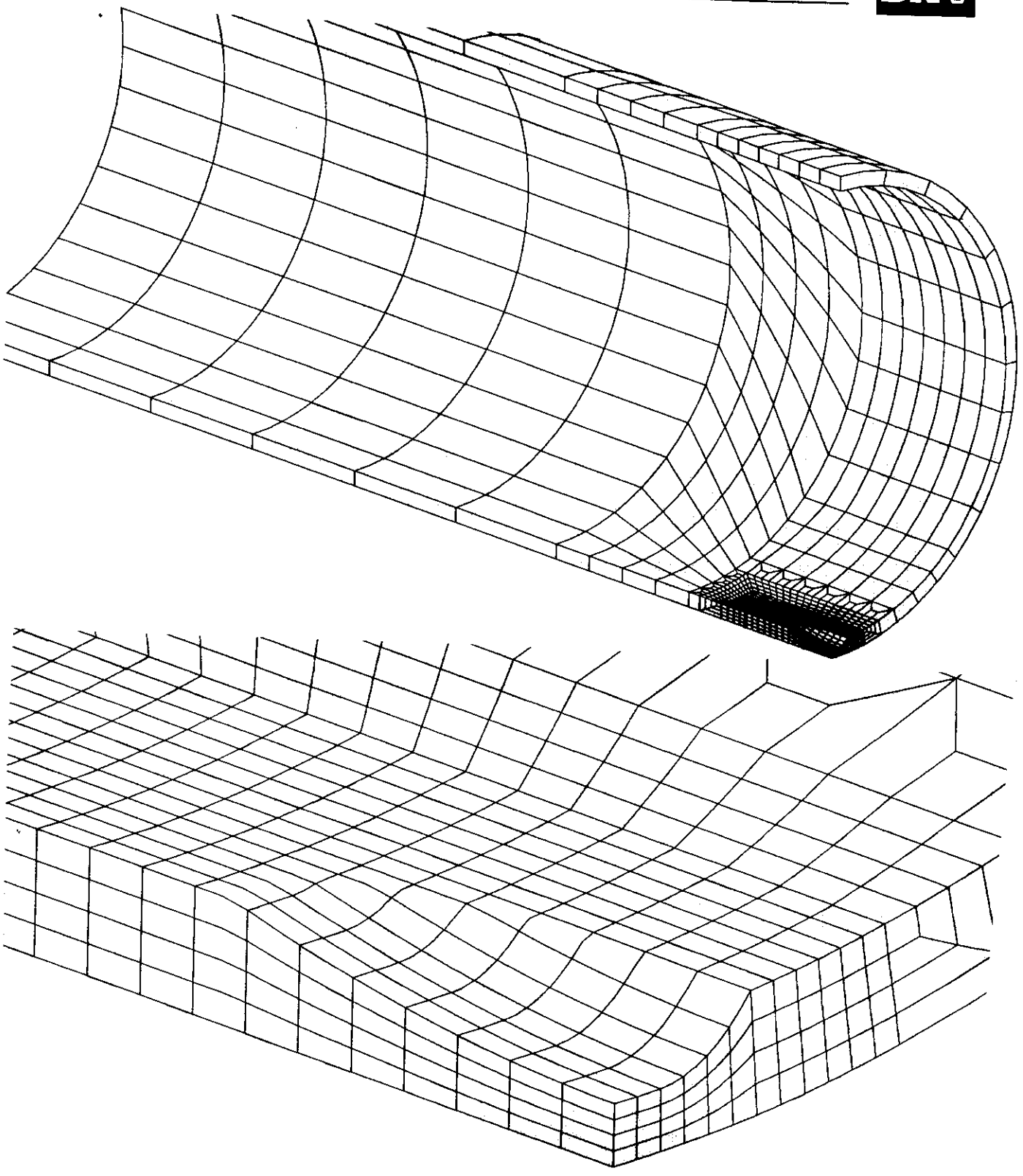

Figure 4-5 Example of model with parabolic shaped corrosion defect

4.1.4 Internal versus external located corrosion

For practical purposes the laboratory test specimens were made with the artificial corrosion defect at the outer surface. For offshore pipelines a corrosion defect is normally located at the internal surface, while for onshore pipelines the defect could as well be at the external surface. Duplicate analyses were made with the same corrosion defect at the external and the internal surface.

The burst capacities from the analyses were the same for internal and external defects.

4.1.5 Defects width

The defect width in the models was in most cases 3 times the wall thickness, but one model was made with a defect width of 15 times the thickness. The burst capacity was close to the same for the narrow and the wide defect for the X60 material. The wide defect had actually just slightly higher capacity than the narrow one.

The model, simulating laboratory test no. 1 was analysed with the material determined with coupon tests. The material curve showed a clear and long yielding plateau. Another analysis was performed to check if the yielding plateau was of significance, and the results showed close to no effect of this. The capacity was the same, even with significant change in the first part of the material curve.

Another pair of analyses were performed, same as the above, but with less width, w/t=3. In this case the same change of capacity was observed as in the sensitivity study. This effect has not been studied in more details, and it is assumed that for wide defect the capacity is mainly dependent on the ultimate strength, and for narrow defects the yield stress also has an influence. The defect length ratio was L/D= 0.75 and the defect depth ratio d/t = 0.50.

The defect width is studied more in detail using 2D models, which is for infinity long corrosion defects.

4.2 2D analyses

4.2.1 Infinite long corrosion

The plain strain 2D models simulates infinity long corrosion defects, and results from the analyses are shown in Figure 4-6. Infinity long corrosion defects is set equal to 1500 mm, for practical purposes, resulting in a dimensionless length of 18, 21 and 26 depending on the different wall thickness. The results from the 2D analyses correspond well with the results from the 3D analyses with long corrosion.

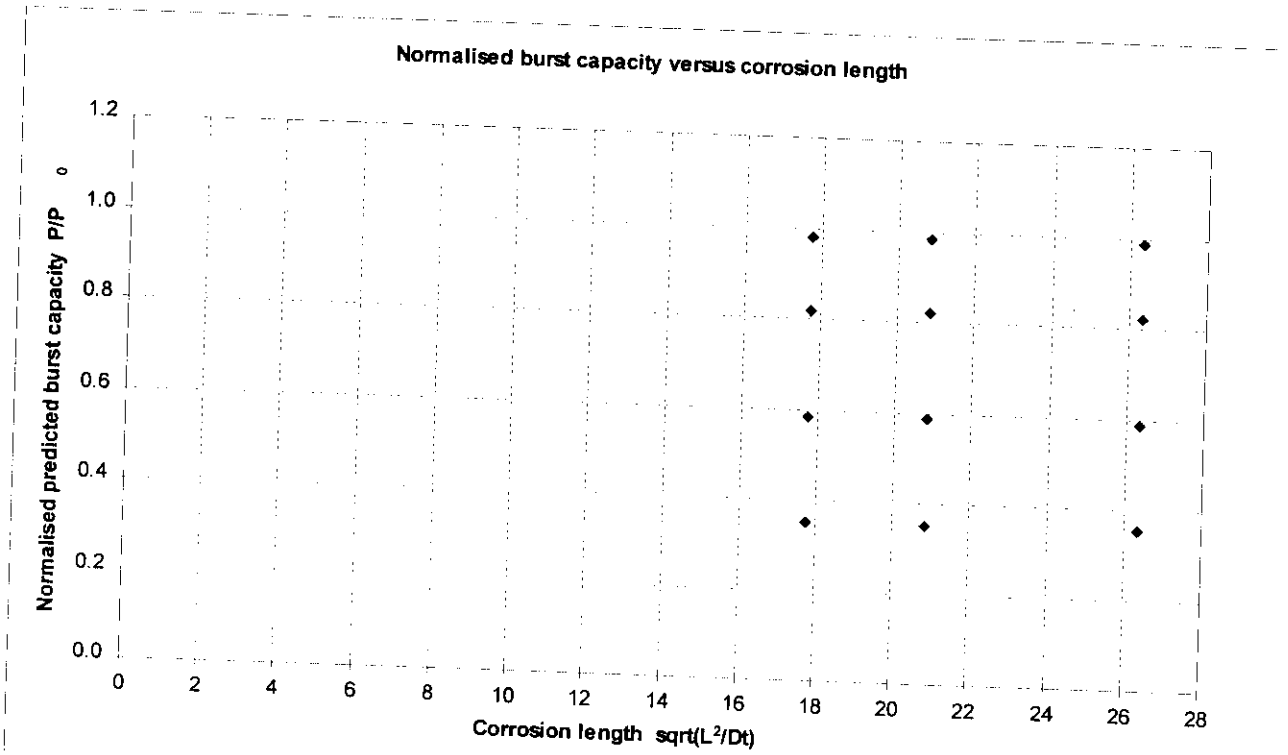

Figure 4-6 Infinity long corrosion defects, plain strain 2D analyses

Table 4-3 Infinity long corrosion defects, plain strain 2D analyses

ID	mm Dia	mm t	mm L	mm d	w/t	Dia/t	L/Dia	d/t	sqrt(L2/(Di	Shape	MPa Yield	MPa UTS	Material	bar P0	bar PC	PC/P0
DNV-P1	324	10	1500.0	1.5	3	32.4	4.63	15 %	26.35	rect.	460	578	X60mm	368.2	363.4	0.987
DNV-P2	324	10	1500.0	3	3	32.4	4.63	30 %	26.35	rect.	460	578	X60mm	368.2	302.8	0.822
DNV-P3	324	10	1500.0	5	3	32.4	4.63	50 %	26.35	rect.	460	578	X60mm	368.2	216.5	0.588
DNV-P4	324	10	1500.0	7	3	32.4	4.63	70 %	26.35	rect.	460	578	X60mm	368.2	129.8	0.353
DNV-P6	324	16	1500.0	2.4	3	20.25	4.63	15 %	20.83	rect.	460	578	X60mm	600.5	591.2	0.984
DNV-P7	324	16	1500.0	4.8	3	20.25	4.63	30 %	20.83	rect.	460	578	X60mm	600.5	492.6	0.820
DNV-P8	324	16	1500.0	8	3	20.25	4.63	50 %	20.83	rect.	460	578	X60mm	600.5	352	0.586
DNV-P9	324	16	1500.0	11.2	3	20.25	4.63	70 %	20.83	rect.	460	578	X60mm	600.5	211	0.351
DNV-P11	324	22	1500.0	3.3	3	14.727	4.63	15 %	17.77	rect.	460	578	X60mm	842.1	827.2	0.982
DNV-P12	324	22	1500.0	6.6	3	14.727	4.63	30 %	17.77	rect.	460	578	X60mm	842.1	688.8	0.818
DNV-P13	324	22	1500.0	11	3	14.727	4.63	50 %	17.77	rect.	460	578	X60mm	842.1	492.8	0.585
DNV-P14	324	22	1500.0	15.4	3	14.727	4.63	70 %	17.77	rect.	460	578	X60mm	842.1	296.3	0.352

4.2.2 Corrosion width and internal versus external corrosion

The internal versus the external corrosion was also studied using 2D models.

Two models with the same dimensions as model P8 in Table 4-3 was made, but with corrosion width w/t = 9, and one with internal corrosion and the other with external corrosion. The one with internal corrosion failed at 347 bar, and the one with external corrosion failed at 342 bar, compared to the failure pressure of 352 bar for the P8 model.

The percentage difference is 1.5 % between the models with internal defect and width w/t equal to 3 and 9. There is another 1.5 % between the failure pressures for the analyses with internal defect and with external defect.

The models are included in Figure 4-7.

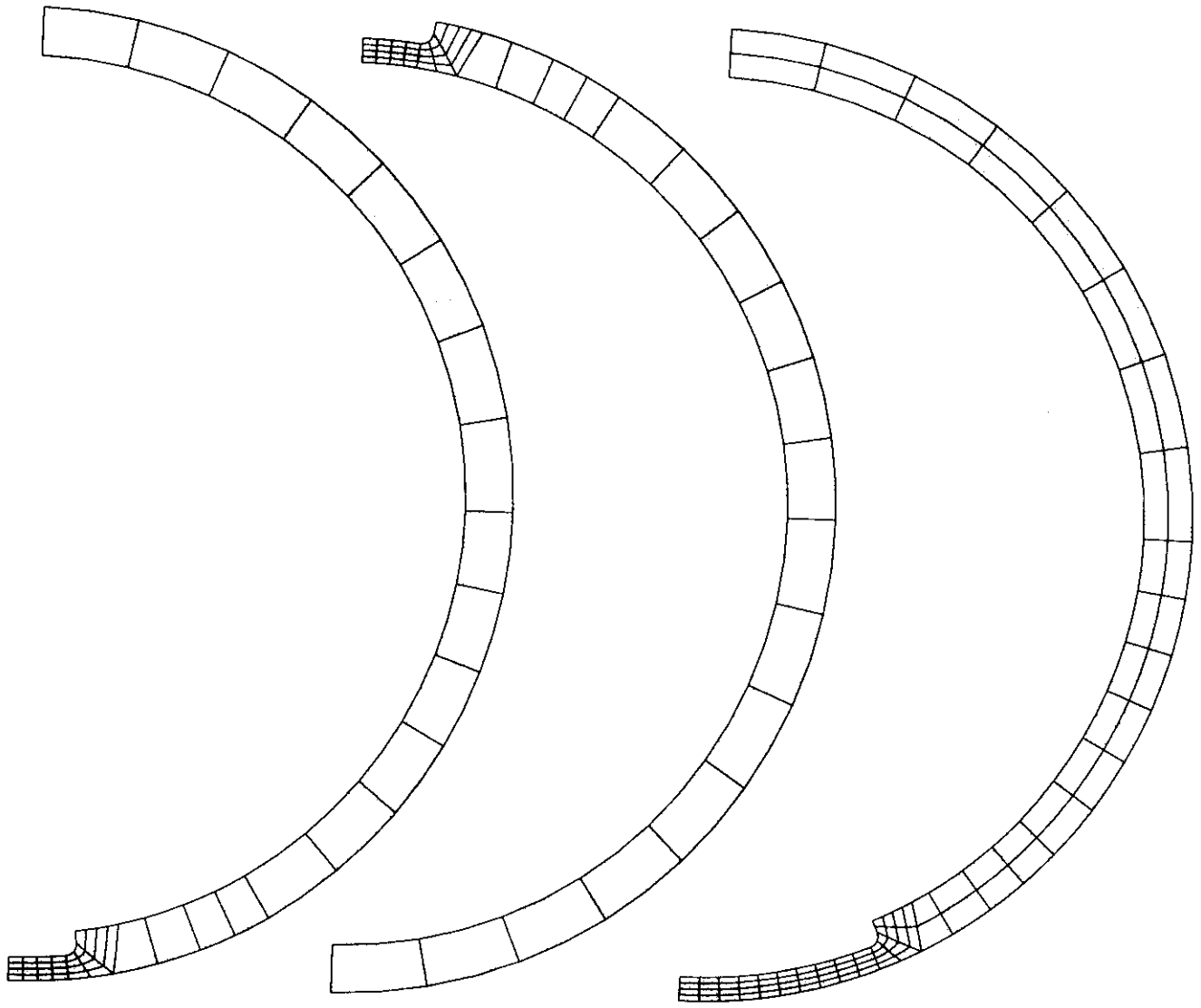

Figure 4-7 2D models, internal versus external corrosion, and width of corrosion.

4.2.3 Mesh density

In the corroded region 4 elements was used through the thickness, which was at a short distance away from the corrosion defect reduced to one element through the thickness. A model equal to the model P8, see Table 4-3 was made with finer mesh. The difference in predicted burst capacity was 0.2 bar which is negligible (and less then the assumed accuracy of the evaluation of the results). The models are included in Figure 4-8.

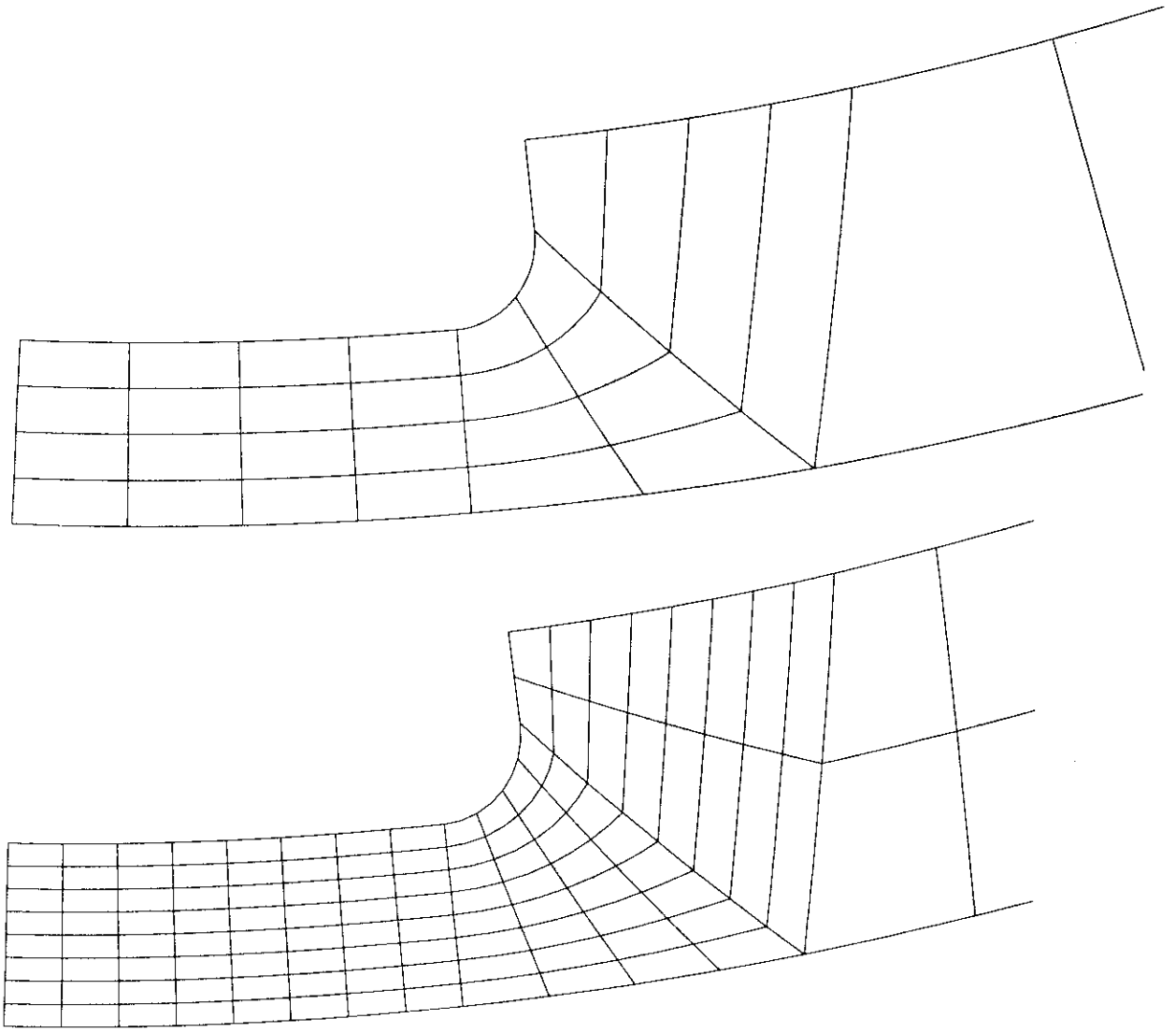

Figure 4-8 2D models, mesh density, close-up view.

5 LONGITUDINAL CORROSION DEFECTS, COMBINED LOADS

5.1 Combined internal pressure and bending moment

5.1.1 Models description

Models used for the study of longitudinal corrosion with internal pressure were modified to also account for bending moment. At the boundary of the models the boundary nodes were restrained to be a stiff plate by using the *EQUATION option in ABAQUS and connect a short beam element to the stiff plate. The beam element was used to in a easy way to apply the load and boundary conditions.

5.1.2 Loading and failure criteria

First the internal pressure were applied to 165 bar, and while keeping the internal pressure constant a bending moment was applied to a predefined level. Further, no keeping the bending moment constant and the internal pressure was increased until failure. If only internal pressure was applied the models failed in the hoop direction as observed for the models with longitudinal corrosion. Three failure criteria were applied, and for high internal pressure there was a minor difference in predicted pressure, 550 MPa, 600 MPa, and numerical instability. One analysis were carried out applying rotation in stead of bending moment, allowing the bending moment to reduce when increasing the internal pressure.

5.1.3 Results

The results from the analyses are shown in Figure 5-10. The internal pressure capacity is reduced with increased bending moment. There is a difference between the various failure criteria, especially when the bending moment increases. The corroded section was located at the compressive side of the bending moment. The load path for one analysis are included, which show the resulting bending moment from an analyses in load displacement control in regard of the rotation/bending moment (always load control for the internal pressure). When increasing the pressure and holding the rotation constant, the bending moment drops. The resulting load path almost overlaps the results from the analyses with the 600 MPa criterion.

The results are compared with results from laboratory tests, and the bending moment capacity and stiffness is much higher in the analyses compared to the tests. The reason for this has not been found. Both the test results and the analyses have been checked, but no full explanation has been found. However, based on our evaluation the results from the laboratory tests seem to be the most correct, and we assume no errors in the instrument recordings in the laboratory tests.

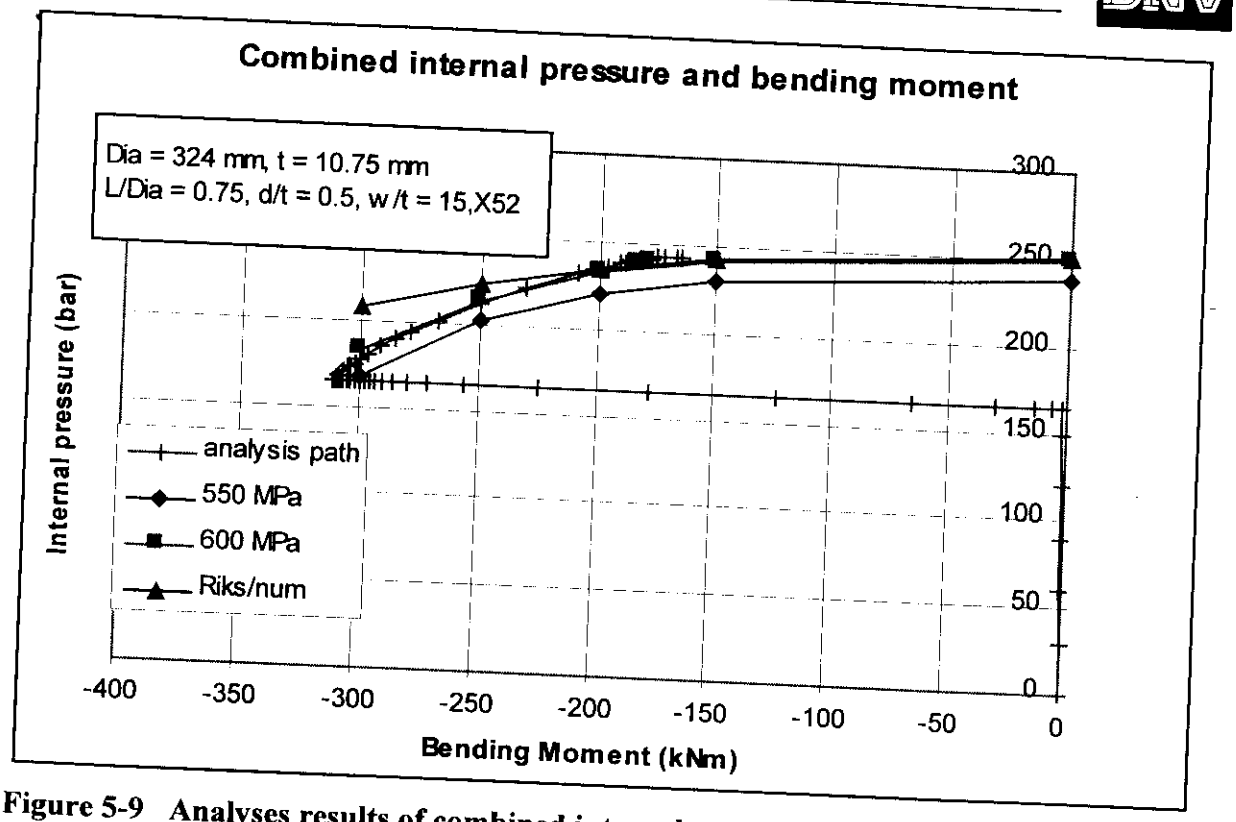

Figure 5-9 Analyses results of combined internal pressure and bending moment.

5.2 Combined internal pressure and axial compressive force

5.2.1 Models description

Models used for the study of longitudinal corrosion with internal pressure were modified to also account for axial compressive force.

5.3 Loading and failure criteria

First the internal pressure were applied to a defined level, and while keeping the internal pressure constant an axial compressive force was applied until failure. If only internal pressure was applied the models failed in the hoop direction as observed for the models with longitudinal corrosion. The burst failure was not observed in the analyses when the internal pressure was at a modest level. When applying axial compressive force this resulted in excessive plastic deformations, without indications on the pipe would have bursted. Three failure criteria were applied, and for high internal pressure there was a minor difference in predicted pressure, 10% strain, stress at UTS and numerical instability. For modest internal pressure and high axial compressive loads the numerical instability was reached before the two other failure criteria were fulfilled. A tensile failure, rupture, was not predicted for modest internal pressure, only excessive yielding was observed.

5.4 Results

The results from the analyses are shown in Figure 5-10. The internal pressure capacity is reduced with increased axial compressive load, but the failure mode is different for high internal pressure and modest internal pressure. The results are compared with the laboratory tests in the project assessment report.

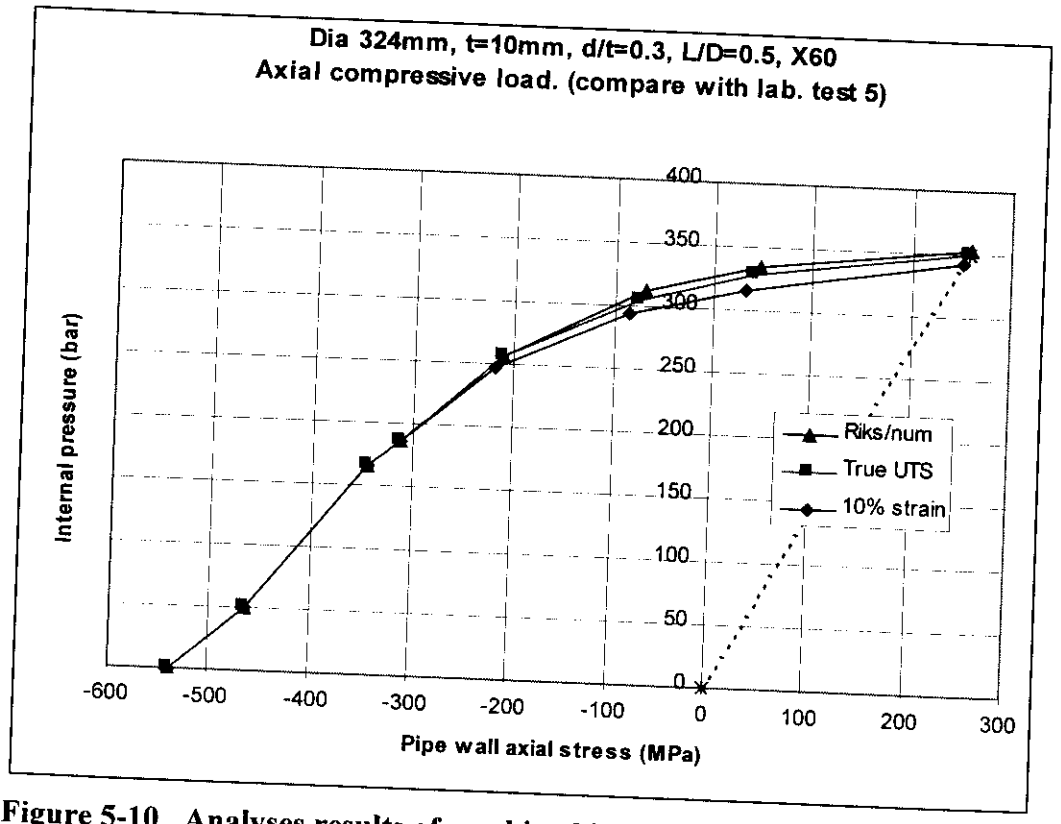

Figure 5-10 Analyses results of combined internal pressure and axial loads

6 CIRCUMFERENTIAL CORROSION DEFECTS, COMBINED LOADS

6.1 Models description

The analyses with circumferential corrosion defects were axis-symmetric models, using 8-noded axis-symmetric 2D elements. Only 2 models were used, and different load sequences were applied to the models, resulting in approximately 15 analyses. The pipe diameter was 324mm, wall thickness 10.4mm, and the actual material properties of the pipe were used. The corrosion defect was in the full circumferential with a longitudinal extent of 12 mm and a depth of 50% and 70% of the wall thickness. The model with 50% corrosion depth is shown in figure #. The model utilise the symmetry of both the load and the geometry, and for an illustration the model with 50% corrosion depth and 70% corrosion depth are mirrored twice in figure # and #. Note that only ¼ of the shown illustrations are the actual model.

6.2 Loading and failure criteria

Several analyses with various load paths of internal pressure and axial load were performed with the two models. First the internal pressure were applied to a defined level, and while keeping the internal pressure constant an axial compressive force was applied until failure. If only internal pressure was applied the models failed in the hoop direction as observed for the models with longitudinal corrosion. The burst failure was not observed in the analyses when the internal pressure was at a modest level. When applying axial compressive force this resulted in excessive plastic deformations, without indications on the pipe would have bursted. When large deformations were observed, approximately 10% strain, the analysis had reached the failure.

6.3 Results

The analyses results are included in figure # for both the 50% and the 70% corrosion depth models. For internal pressure only and not including the end cap force, the predicted capacity is almost identical for the 50% and the 70% corrosion depths. This illustrates that the load carrying capacity is in the hoop direction and that the pressure load in the corrosion defect is carried by the adjacent material. For a thin wall pressure container the axial stress is half the hoop stress (internal pressure loading only). In case of a full circumferential corrosion defect of 50% of the wall thickness, the axial stress in the corroded cross section has to carry the same load and hence the axial stress is increased to twice compared to the uncorroded section. In this case the axial stress in the corroded section is equal to the hoop stress in the uncorroded pipe. In this case it is expected that the capacity for a rupture due to the axial stress is close to the same as for a rupture due to the hoop stress. In case of 70% corrosion depth the axial stress in the corroded section exceeds the hoop stress in the uncorroded pipe by a factor of 1.66. It is therefore expected that the pipe will rupture due to axial tensile stress in the corroded section long before rupture due to the hoop stress, see the drop in the capacity curve for the 70% corrosion defect for tensile axial stress.

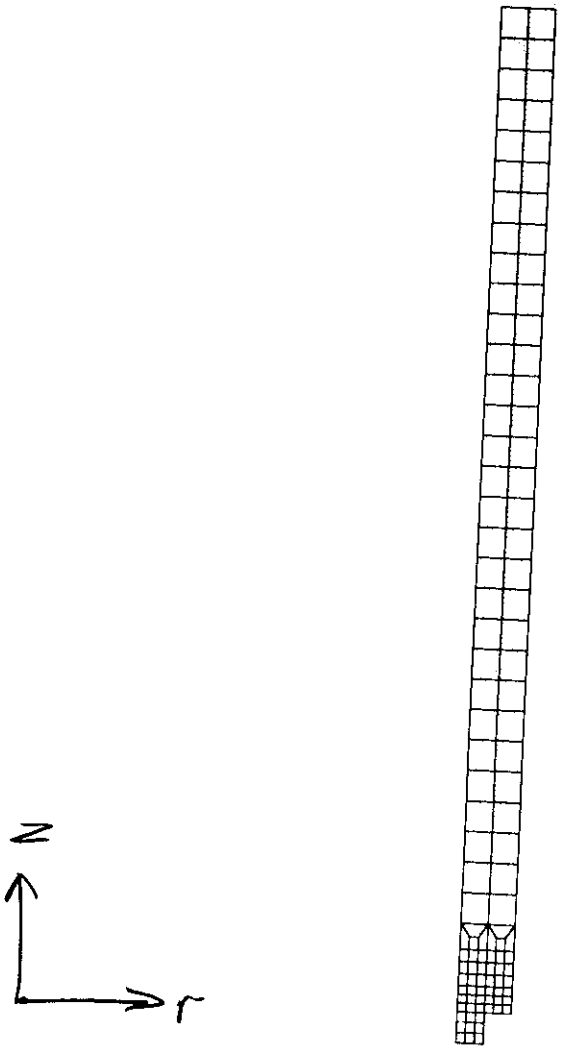

Figure 6-11 FE model of circumferential corrosion, 50% corrosion defect.

Accordingly, for compressive axial stress, the axial capacity will be exceeded before the hoop stress capacity for modest internal pressure and large axial compressive forces. Different from tensile stresses, the compressive stresses will only result in excessive deformations and no rupture. However, the large deformations also results in rotations and local bending of the pipe wall which also results in tensile stresses which could induce rupture.

The failure criterion is 10% strain in the corroded section. Two examples of exceeding the 10% criterion is indicated, where the one for 50% corrosion depth and 300 bar were analysed all to 70% strain.

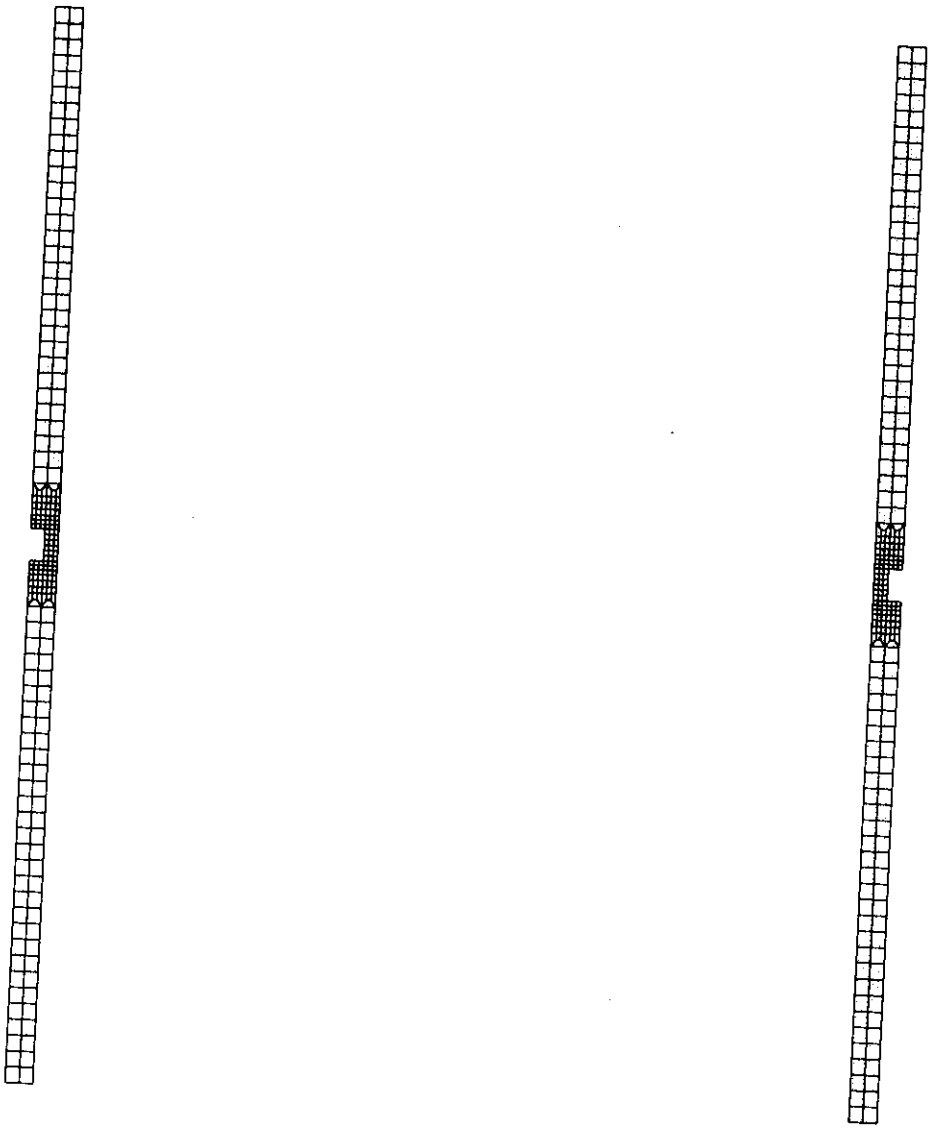

Figure 6-12 Illustrative view of the model with 50% corrosion depth. Only ¼ of the shown elements are used in the finite element analyses, see previous figure.

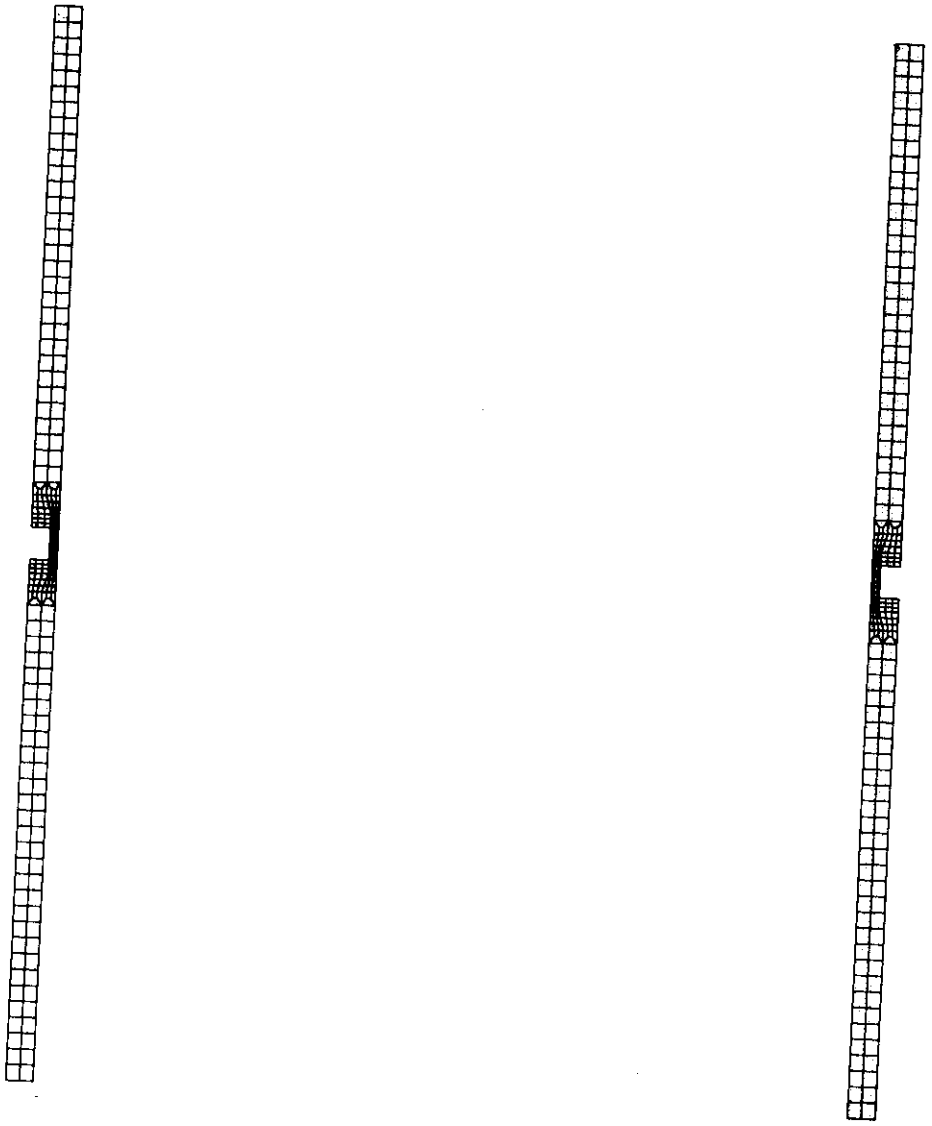

Figure 6-13 Illustrative view of the model with 70% corrosion depth. Only ¼ of the shown elements are used in the finite element analyses.

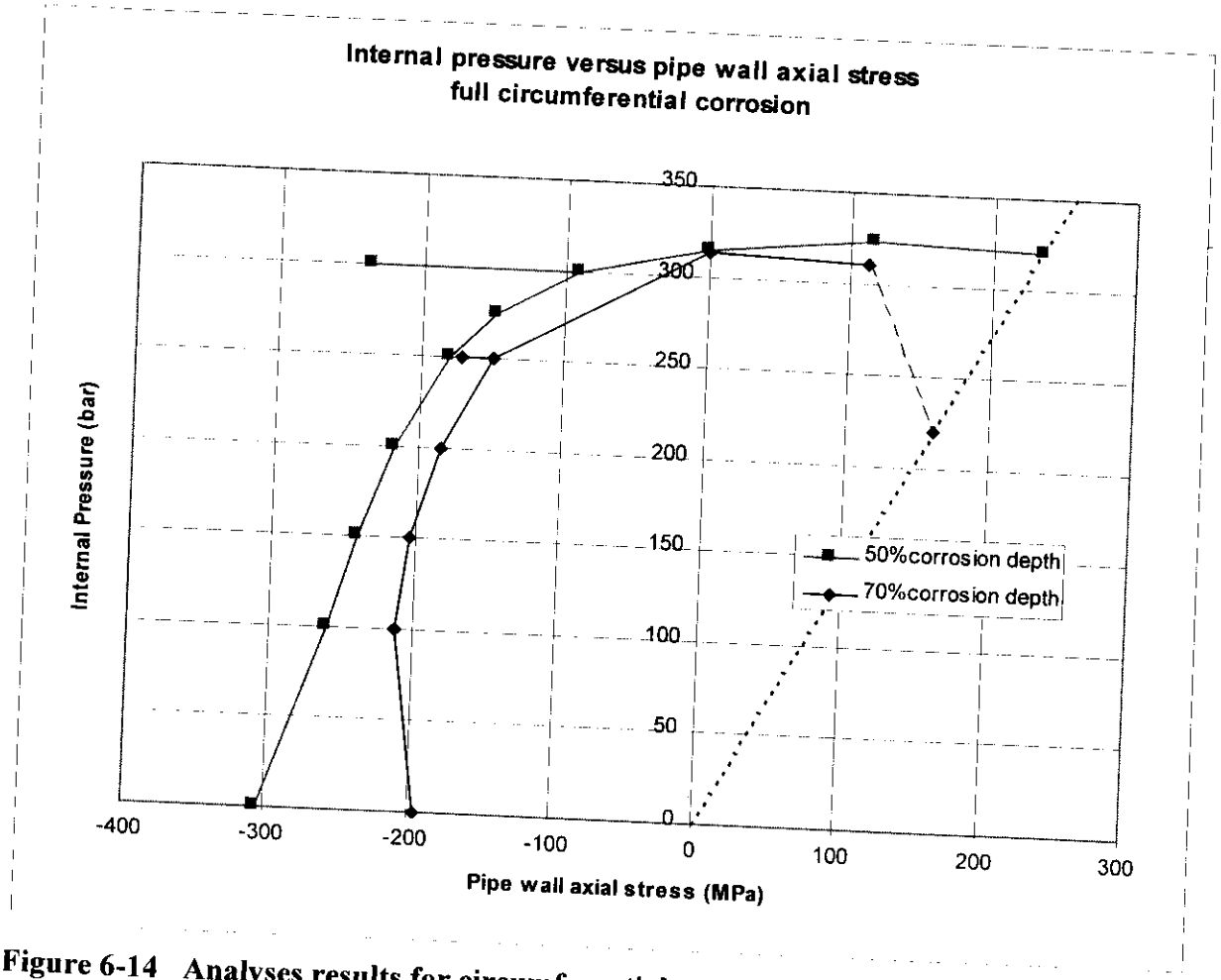

Figure 6-14 Analyses results for circumferential corrosion defects.

7 REFERENCES

ABAQUS v 5-4 (1995), Hibbitt, Karlsson and Sorensen, Providence, Rhode Island, USA

Fu ,B. and Kirkwood, M. G. (1995), "Predicting Failure Pressure of Internally Corroded Linepipe using the Finite Element Method", Offshore Mechanics and Arctic Engineering, OMAE'95, Copenhagen

- o0o -